Tampere University

Jenni Keränen

# AN ORGANOID METHOD AS A MODEL FOR RETINAL PIGMENT EPITHELIUM MATURATION

Faculty of Medicine and Health Technology
Master's thesis
April 2023

# ABSTRACT

Jenni Keränen: An organoid method as a model for retinal pigment epithelium maturation
Master's thesis
Tampere University
Master´s Programme in Biomedical Technology
Supervisors: Prof. Heli Skottman, MSc Viivi Karema-Jokinen
Examiners: Prof. Vesa Hytönen, Prof. Heli Skottman
April 2023

**Background and Aims:**
The retina is a layer of neural cells and photoreceptors located at the back of the eye. Its responsibilities include detecting the light entering the eye and conveying the produced message to the optic nerve, and finally the brain. Retinal pigment epithelium (RPE) is a single layer of pigmented epithelial cells located beneath the photoreceptors. The main roles of the RPE are focused on the maintenance of the retina and especially the photoreceptors by e.g., transepithelial transport, absorption of scattered light, and secretion of growth factors. Faults in the RPE quicky result in various retinal diseases including age-related macular degeneration and retinitis pigmentosa, both of which lack treatment options partially due to the limitations of the current RPE cell models, including the challenge of achieving mature *in vitro* RPE.
A culturing protocol for optic vesicle-containing brain organoids was published by Gabriel et al. at the end of 2021. The brain organoids spontaneously developed bilateral optic vesicles, which included the RPE together with the developing components of the neural retina. In the human eye, the RPE and the retina are in close cooperation already during their development. Therefore, the presence of the neural retina in the organoids could improve the maturation of the RPE. Thus, this thesis aimed to differentiate viable optic vesicle -containing brain organoids as an improved model for RPE maturation to be utilized in eye and especially RPE-related research.

**Methods:**
The human embryonic stem cell line Regea 08/017 was used for the differentiation of the organoids. The organoid differentiation was conducted as in the original protocol by Gabriel et al. (2021), with the exception of choosing to culture the organoids on ultra-low adhesion well plates instead of spinner flasks. The organoids were collected for characterization experiments on days 20, 50 and 60. The morphology and cellular content of the optic vesicles were characterized through gene expression analyses and immunocytochemistry.

**Results and Conclusions:**
The differentiation of the optic vesicle-containing brain organoids from the Regea 08/017 human embryonic stem cells was successful with slightly modified methods compared to the original publication by Gabriel et al. (2021). Characterizations revealed the gene expression of early eye development genes in addition to genes related to the RPE and components of the neural retina. Immunocytochemistry experiments showed the inner morphology of the optic vesicles, from which the presence of RPE cells could be determined. However, the maturity of the RPE could not be accurately determined. For proper maturity experiments, the RPE should be extracted from the organoid structures and cultured further individually.

Keywords: retina, retinal pigment epithelium, RPE, organoid, retinal organoid, brain organoid

# PREFACE

This Master of Science thesis was conducted jointly in Prof. Heli Skottman's Eye Regeneration and Dr Soile Nymark's Biophysics of the Eye research groups at the Faculty of Medicine and Health Technology at Tampere University. I would like to thank Prof. Heli Skottman and Dr Soile Nymark for providing me with an interesting research topic and guidance throughout the process. Additionally, I would like to extend my thanks to Dr Nemanja Milicevic, MSc Viivi Karema-Jokinen, and the Eye Regeneration group laboratory technicians Hanna Pekkanen and Outi Melin for their guidance and assistance in the experimental part of this thesis.

The author acknowledges the Tampere Imaging Facility (TIF) for their service.

Tampere, 17 April 2023

Jenni Keränen

# CONTENTS

# LIST OF SYMBOLS AND ABBREVIATIONS

| | |
|---|---|
| 2D | two-dimensional |
| 3D | three-dimensional |
| AMD | age-related macular degeneration |
| AMPK | AMP-activated protein kinase |
| ARPE-19 | adult RPE-19 |
| BEST1 | bestrophin-1 |
| BMP | bone morphogenetic protein |
| $Ca^{2+}$ | calcium ion |
| $Ca_V$ | voltage-gated calcium channel |
| $Cl^-$ | chloride ion |
| Cl-19 | claudin-19 |
| CRALBP | cellular retinaldehyde-binding protein |
| Cx36 | connexin 36 |
| Cx43 | connexin 43 |
| EB | embryonic body |
| ECM | extracellular matrix |
| ESC | embryonic stem cell |
| FGF | fibroblast growth factor |
| hESC | human embryonic stem cell |
| IPM | interphotoreceptor matrix |
| iPSC | induced pluripotent stem cell |
| IRBP | interphotoreceptor retinal binding protein |
| $K^+$ | potassium ion |
| MITF | microphthalmia-associated transcription factor |
| $Na^+$ | sodium ion |
| $Na_V$ | voltage-gated sodium channel |
| OC | optic cup |
| OV | optic vesicle |
| OVB | optic vesicle-containing brain organoid |
| PEDF | pigment epithelium-derived factor |
| POS | photoreceptor outer segment |
| RA | retinyl acetate |
| RGC | retinal ganglion cell |
| RO | retinal organoid |
| RP | retinitis pigmentosa |
| RPC | retinal progenitor cell |
| RPE | retinal pigment epithelium |
| RPE65 | retinoid isomerohydrolase retinal pigment epithelium 65 kDa protein |
| SHH | Sonic hedgehog signalling |
| TEER | trans-epithelial electrical resistance |
| TGF-$\beta$ | transforming growth factor $\beta$ |
| TJ | tight junction |
| VEGF | vascular-endothelial growth factor |
| ZO | zonula occludens |

# 1. INTRODUCTION

Our vision is a vital and complex sense produced together in cooperation by the eyes and the brain. When the light passes through the cornea and the lens, it's focused on the light-sensitive retina at the back of the eye. When excited by light, the photoreceptor cells at the back of the retina convey their proportional response to the neuronal cells of the retina, which then enhance and direct the message to the brain via the optic nerve. (Schwab, 2011) The work done by the photoreceptors is supported by the retinal pigment epithelium (RPE), a monolayer of pigmented hexagonal epithelial cells located between the outer segments of the photoreceptors and Bruch's membrane (Strauss, 2005).

RPE has many tasks vital to the proper function of the photoreceptors such as the absorption of scattered light and shielding against photo-oxidation, phagocytosis of the photoreceptor outer segments, transport of nutrients, and the conversion of all-*trans*-retinal back to 11-*cis*-retinal in the visual cycle. (Strauss, 2005) The significance of functional RPE to the photoreceptors and the whole retina is highlighted by issues that arise in the case of non-functional RPE. Dysfunction of the RPE is linked to many vision-related illnesses, such as age-related macular degeneration (AMD) and retinitis pigmentosa (RP). For example, AMD is the leading cause of blindness in elder adults worldwide but its treatment options are still limited. (Nashine, 2021)

RPE models are required for the research of the disease mechanisms and possible treatments, such as graft transplants and gene therapies. Currently, the two-dimensional (2D) models of RPE are well established (Engelmann and Valtink, 2004; Lakkaraju et al., 2020), but do not always take into account the complex interactions between the RPE and its surrounding tissues, and their effects on the maturation of the RPE. Attempts to co-culture RPE with e.g. adult neurosensory retina (Kaempf et al., 2008), and RPE culturing scaffolds mimicking Bruch's membrane (Xiang et al., 2014) have been investigated as solutions, but the attention has now been moved towards three-dimensional (3D) cell culture models. Retinal organoids (ROs) are 3D structures derived from stem cells that include the cell types and the ultrastructure of a retina. Various viable RO models have been developed (Capowski et al., 2019; Fligor et al., 2018; Regent et al., 2020) but they share the same characteristic issues. The culturing protocols are noticeably time-consuming and expensive, with the formation of ROs often taking at least 100 days (Li et al.,

2021). In addition, the RPE in the ROs is often amiss or appears as separate patches instead of being in close connection to the rest of the retinal cells (Cowan et al., 2020; Isla-Magrané et al., 2021).

In 2021, Gabriel et al. published a protocol for human brain organoids with forebrain-like regions that spontaneously assemble functional bilateral optic vesicles (OVB-organoids). The optic vesicles of the organoids derived from induced pluripotent stem cells (iPSCs) establish the cellular components of a naturally developing optic vesicle, including primitive corneal epithelial and lens-like cells, RPE and retinal progenitor cells. (Gabriel et al., 2021) The organization of the immature neural retina occurred within 60 days, which is parallel to the development of the human embryo (Gabriel et al., 2021; Sadler and Langman, 2012). This thesis aims to differentiate viable OVB-organoids as described by Gabriel et al. (2021) as a model for RPE maturation. The thesis begins with a literature review of the general structure and function of both the retina and the RPE, followed by a discussion of RPE dysfunction and currently utilized RPE models. In the experimental part, the generation of the OVB-organoids and their characterization are described. In the end, the results are discussed, and the experimental part is concluded.

# 2. LITERATURE REVIEW

## 2.1 The human eye

The human eye consists of several layers. The sclera forms the outer protective layer of the eye and becomes contiguous with the cornea at the limbus. The cornea opposed to the sclera is a clear and steeply curved structure. The curved surface of the cornea refracts the entering light to the lens, a clear, curved structure kept in place by long fibers called zonules. The lens refracts the entering light further and focuses it to the retina, the innermost layer of the eye. In the centre of the eye lies a large fluid-filled space called the vitreous cavity, which takes part in magnifying the image reflected to the retina. (Sadler and Langman, 2012; Schwab, 2011)

The inner part of the sclera is split into three additional zones: the choroid, the iris and the ciliary body. The choroid lies beneath the retina supplying it with nutrients. The iris is located anteriorly to the retina, and the ciliary body lies behind the iris. The ciliary body produces fluid for the interior of the eye and maintains the pressure within the eyeball. (Schwab, 2011)

The photoreceptors of the retina form the outmost layer of the retina with two types of photoreceptor cells present: the dim light vision specialized rods and the bright light vision specialized cones. An increased concentration of cells in the macula with primarily cone photoreceptors correlates with high visual acuity and colour vision. Thus, the macula and especially its' centre, the fovea, are areas providing sharp vision. The optic disc, where the optic nerve exits the eye, is located near the macula. The surface of the optic disc is bare of photoreceptors, which renders it a blind spot. (Sadler and Langman, 2012; Schwab, 2011) The structure and function of the retina will be discussed in more detail later. See Figure 1 for the visual summary of the basic structure of the human eye.

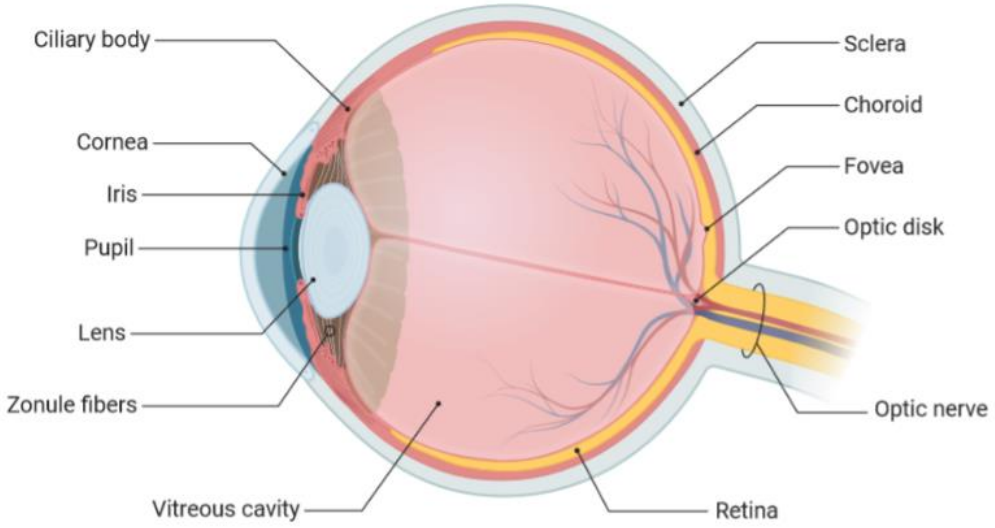


***Figure 1**. The basic structure of the human eye. Adapted from "Anatomy of the Human Eye", by BioRender.com (2023). Retrieved from https://app.biorender.com/biorender-templates.*

### 2.1.1 Optic vesicles

During the fourth week of embryonic development, the developing eyes appear as grooves on the sides of the forebrain. The positioning of the grooves is controlled by the symmetrical separation of the eye field, a field of neuroectodermal cells acting as the origin point for eyes, driven by sonic hedgehog (SHH) signalling (Sadler and Langman, 2012). The eye field itself is established by the master gene *PAX6* and its regulatory target *SOX2* in the anterior neural ridge of the neural plate (Sadler and Langman, 2012) after the anterior-posterior and dorso-ventral patterning of the anterior neural tube (Diacou et al., 2022).

The evagination of the forebrain grooves leads to the formation of two symmetrical optic vesicles (OVs). Interactive signalling between the OVs and the surrounding mesenchyme initiates further evagination of the OVs with the surface ectoderm-derived lens-placode leading to the formation of two double-layered optic cups (OCs). The secretion of fibroblast growth factor (FGF) from the surface ectoderm promotes the development of the neural retina from the inner layer of the OCs (Diacou et al., 2022; Sadler and Langman, 2012). Meanwhile, the Wnt/β-catenin pathway (Westenskow et al., 2009), transforming growth factor β (TGF-β), and especially their downstream products microphthalmia-associated transcription factor (MITF) and orthodenticle homeobox 2 (OTX2), secreted by the surrounding mesenchyme drive the development of retinal pigment epithelium from the outer OC layer. (Sadler and Langman, 2012)

## 2.2 The retina

The retina consists of three cell layers, and two additional layers: the outer nuclear layer, the inner nuclear layer, the retinal ganglion cell (RGC) layer, and the inner and outer plexiform layers. Each cell layer consists of the bodies of various neural cells, which contribute to the detection of the entering light and the progression of the produced signal. The synapses of the neural cells are largely located in the plexiform layers. (Schwab, 2011) In addition, the retina contains a large number of supporting neural cells called the Müller glia. The cell bodies of the Müller glia are located in the inner nuclear layer, while their processes span the whole neural retina. They maintain the structure and function of the retina by, for example, mediating neurotransmitters and ions. (Newman and Reichenbach, 1996)

The photoreceptors are located in the outer nuclear layer of the retina. The photoreceptor cells, rods and cones, receive the photons from the light entering the retina and transform the signal into electrical impulses, which are forwarded to the bipolar layer. (Kolb, 2012) The RPE located right under the photoreceptor layer oversees the upkeep of the photoreceptor cells (Strauss, 2005). It, alongside Bruch's membrane, will be discussed in more detail later.

The inner nuclear layer contains three types of cells including amacrine, bipolar and horizontal cells (Schwab, 2011). Horizontal cells lie at the outer plexiform layer, where a dense population of synapses between the dendrites of the horizontal cells connect to the photoreceptors (Kolb, 2007a). Similarly, the amacrine cells are located at the inner plexiform layer, where they form synapses with the ganglion cells (Kolb, 2007b). The bipolar cells lie in the middle of the bipolar layer with connections to both the photoreceptors and the retinal ganglion cells (Schwab, 2011). The electrical signals originating from the photoreceptors are forwarded through the inner nuclear layer to the RGCs which are located in the innermost layer of the retina. RGCs collectively transmit the image-forming and non-image-forming signals as action potentials through the optic nerve to the brain, where the final image is formed. (Schwab, 2011; Sernagor et al., 2001) See Figure 2 for a visual summary of the structure of the retina.

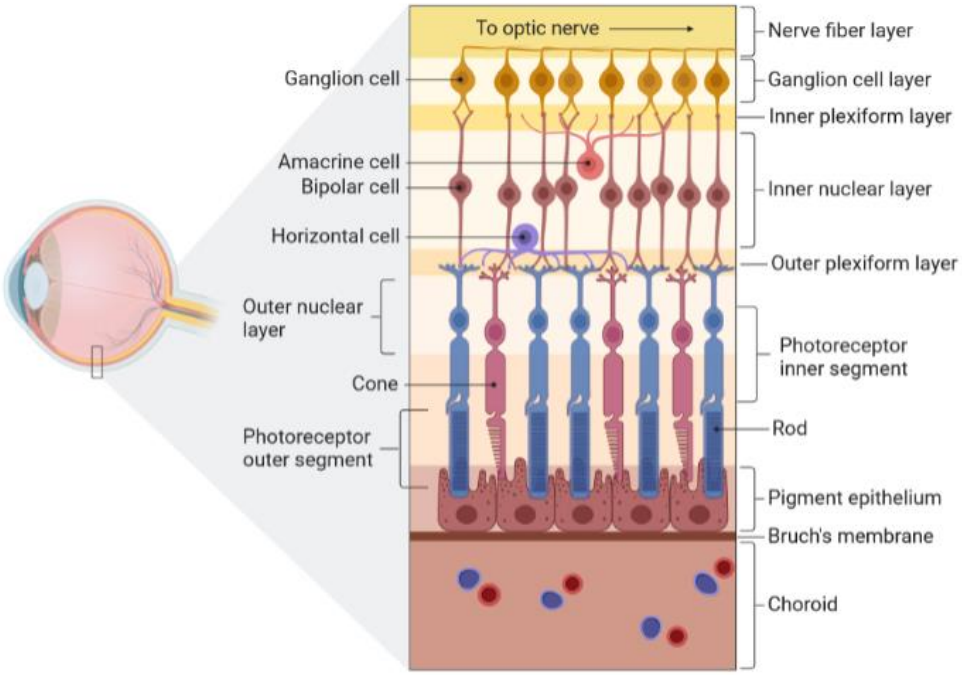


***Figure 2**. The structure of the human retina. Müller glia are not depicted in the figure for clarity. Adapted from "¨Structure of the Retina", by BioRender.com (2023). Retrieved from https://app.biorender.com/biorender-templates.*

The inner layer of the optic cups differentiates into the neural retina during embryogenesis. (Diacou et al., 2022) The retinal progenitor cells (RPCs) of the neural retina give rise to the many cell types of the retina. The development order of the retinal cell types is well preserved with amacrine, horizontal, and cone photoreceptor cells being the first to differentiate. Rod photoreceptors, bipolar cells and Müller glia follow suit. (Cepko, 2014) The inner and outer layers of the optic cups are separated by a thin layer, which is eventually filled by the interphotoreceptor matrix (IPM), a type of extracellular matrix (ECM) synthesized by the developing photoreceptors and the RPE (Strauss, 2005). The IPM partakes in the development and maintenance of the photoreceptors through e.g. regulating oxygen, nutrient, and growth factor transport, while simultaneously serving as a vessel for the retinal adhesion to the RPE. (Ishikawa et al., 2015; Röhlich, 1970). Due to its specialized function, the composition of the IPM differs from the usual ECM. In addition to the presence of various specialized proteins and growth factors, retinoic acid and fatty acids are found in the IPM. On the other hand, the IPM lacks collagen, elastin and fibrillin found in the basic ECM. (Ishikawa et al., 2015) The outer layers of the OCs differentiate into the RPE. The formation of the IPM contributes to the maturation of the RPE. (Ishikawa et al., 2015; Strauss, 2005) The structure and function of the RPE will be discussed in more detail next.

## 2.3 Retinal pigment epithelium

RPE is a monolayer of hexagonal epithelial cells located between the photoreceptors and the choroid of the eye, where the RPE acts as a part of the blood-retinal barrier, a barrier between the choroidal blood supply and the neural retina. (Strauss, 2005) The cytoskeleton of the RPE consists of microfilaments, microtubules, and intermediate filaments composed of actin, tubulin, and fibrous proteins, respectively. The filaments give the individual cells their shape while similarly connecting the epithelium through tight junctions (TJs) and adherence junctions. (Bonilha, 2014)

The RPE's apical, IPM-facing surface is covered in long microvilli maximising the apical surface area and interacting with the outer segments of the photoreceptors (Röhlich, 1970). Bundles of actin filaments bound by actin-binding proteins such as ezrin localize in the microvilli (Kivelä et al., 2000). The basal surface of the RPE is highly infolded and lies on the Bruch's membrane, an ECM rich in e.g. elastin and collagen (Booij et al., 2010). Ezrin can be found in the infoldings as well, alongside actin filaments and $\alpha$-actinin (Arikawa and Williams, 1991; Bonilha et al., 1999). The apical-basolateral polarity is typical for epithelium, including the RPE, and is the basis for many of the tissue's functions. The polarity is maintained by the tight junctions, cell-cell junctions present in the apical region of epithelial cells. (Alberts et al., 2015) TJs are discussed in more detail later in relation to the polarity of the RPE.

As the name states, RPE is a pigmented tissue. The three major types of pigment granules present in the RPE are melanosomes, lipofuscin and melanolipofuscin. Melanosomes synthesize the pigment molecule melanin, which is used for the absorption of scattered light. (Barral and Seabra, 2004) Melanosomes are formed during embryogenesis, while lipo- and melanolipofuscin granules are formed in the RPE from the undigested photoreceptor outer segments (POS). They accumulate in the tissue with age and can cause RPE dysfunction later in life. (Biesemeier et al., 2011)

### 2.3.1 Development and maturation

After the formation of the IPM, the RPE begins its development process. The Wnt/$\beta$-catenin pathway, TGF-$\beta$, and their downstream targets transcription factors OTX2 and MITF are critical for the differentiation of the RPE from the outer layer of the optic cup (Fujimura et al., 2009; Westenskow et al., 2009). MITF activates the tyrosinase promoter, which results in melanogenesis and the neuroectoderm of the outer layer beginning to

differentiate into RPE (Ma et al., 2019) with the assistance of other factors such as retinoic acid released from the embryonic retina. Retinoic acid is also being exchanged between the developing RPE and neural retina through the IPM. (Strauss, 2005) The transfer is mediated by the interphotoreceptor retinal binding protein (IRBP), a crucial factor in the visual cycle as well, as discussed later (Rando, 2001). The polarity of the RPE develops alongside the maturation of the tight junctions. When the apical-basolateral polarity of the tissue has been established, the accompanying maturation of the RPE cytoskeleton results in the apical microvilli elongation. (Strauss, 2005)

After the initial differentiation steps, the RPE begins close cooperation with the developing photoreceptors. The primordial photoreceptors begin to differentiate and extend their outer segments, to which the RPE responds by elongating the apical microvilli even further and surrounding the POS. While the apical side of the RPE goes through the final maturation processes, the basal infoldings deepen and reach their mature form as well. (Strauss, 2005) Ezrin is required in both processes (Bonilha et al., 1999) thus acting as a marker of RPE polarization and its development (Kivelä et al., 2000). Further, the apically located microtubule-based primary cilia seem to have an important part in the maturation of the RPE. During the maturation process, the primary cilia have been reported to regulate the Wnt/β-catenin pathway, for example. (May-Simera et al., 2018) Fully mature RPE contains only a few primary cilia highlighting their importance during the development phase (Sun et al., 2021). While mature RPE can be detected around 8 weeks *in vivo*, photoreceptor maturation can take up to hundreds of days (Johansson et al., 2019; Regent et al., 2020). Regardless, the maturation of the photoreceptors is dependent on the RPE, and vice versa (Sheedlo et al., 1998).

### 2.3.2 Polarity

Many of the RPE's functions, such as electrical signalling and nutrient transport, require clear distinction in ion channel, transporter and receptor localization between the apical and basolateral domains. (Marmorstein, 2001) The RPE's cellular organelles are localized in a polarizing manner as well. For example, the nuclei localize basally, while the melanosomes required for the absorption of scattered light are localized apically (Khristov et al., 2018).

In addition to the structural differences, the polarity of the RPE is distinguished by the differences in the protein localization between the apical and basolateral domains (Lehmann et al., 2014). For example, bestrophin-1 (BEST1), a calcium-activated chloride channel, is localized at the basal membrane where it partakes in the regulation of the

RPE's intracellular calcium signalling and cell volume (Esumi et al., 2009; Marmorstein et al., 2000). Certain cargo-specific transporters are found more often on the apical or the basolateral membrane, such as the large neutral amino acids transporter 1 (LAT1) and putative sodium-coupled neutral amino acid transporter 7 (SNAT7), respectively (Hellinen et al., 2019).

The different membrane structures are confined to their domains by tight junctions (TJs), cell-cell junctions composed of the tight junction -proteins such as claudins, especially claudin-19 (Cl-19), junctional adhesion molecules (JAMs), occludins, and zonula occludens (ZO) 1 and 2. TJs form belt-like structures around the epithelial cells joining them together by linking the actin cytoskeletons of the adjacent cells. (Alberts et al., 2015) The junctions prevent the free diffusion of molecules between the apical and basolateral domains and between the cytosols of the RPE cells. In addition, they are important regulators of the barrier function of the epithelium by regulating the passage on the paracellular paths. (Otani and Furuse, 2020) The passage between the cells can be measured with trans-epithelial electrical resistance (TEER), a method which measures the transcellular resistance when current is passed through the cells on the trans- and paracellular paths. TEER is widely used in assessing the integrity of the TJs and thus the RPE's barrier function. (Chen et al., 2015) TJs are accompanied by adherence junctions, which form similar belt-like structures just below the TJs. Together with TJs, adherence junctions take part in the mechanical signalling of the cells. (Angulo-Urarte et al., 2020)

## 2.4 Retinal pigment epithelium function

Retinal pigment epithelium has many roles vital for the upkeep of the photoreceptors and the whole retina. It partakes in POS phagocytosis, light absorption, the visual cycle, epithelial transport, and growth factor secretion. (Strauss, 2005) The RPE transports ions and excess water from the subretinal space to the Bruch's membrane while bringing nutrients, such as glucose, in the other direction (Gallemore et al., 1997). The apically located $Na^+$-$K^+$-ATPase provides the energy required for the transepithelial transport (Marmorstein, 2001; Miller et al., 1978) assisted by the other ion channels and transporters located both apically and basolaterally as discussed before.

By secreting various growth factors and proteins, including FGF, vascular-endothelial growth factor (VEGF) and pigment epithelium-derived factor (PEDF), the RPE can help develop and maintain the structure of the retina, and the underlying Bruch's membrane. (Kay et al., 2013) Further, the secreted immunosuppressive and immunoregulatory factors are utilized in the upkeep of the immune privilege of the eye (Ishida et al., 2003).

The remaining functions are discussed in more detail below after the electrical properties. Figure 3 summarizes the function of the RPE.

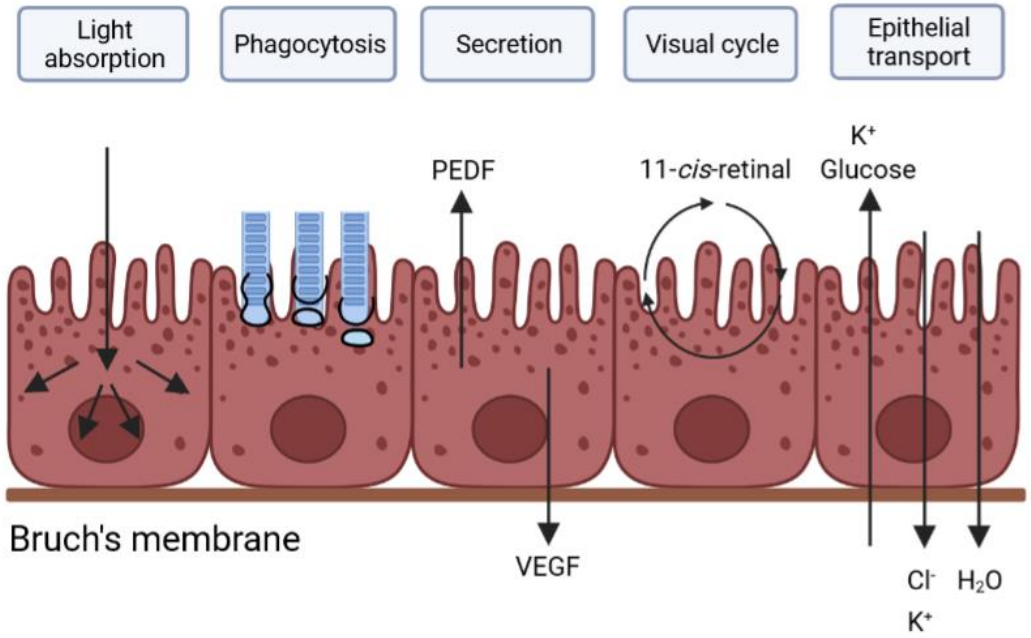


***Figure 3.*** *Graphical summary of the function of the RPE. Modified from Strauss 2005. Created with BioRender.com.*

### 2.4.1 Electrical properties

RPE cells express various voltage- and ligand-gated ion channels on their membranes conducting ions such as sodium ($Na^+$), calcium ($Ca^{2+}$), potassium ($K^+$), and chloride ($Cl^-$). The ion channels serve their purpose of defining the RPE's physiology and regulating its function. For example, the transport of ions across the cell membrane is used to regulate cellular volume and pH. (Wimmers et al., 2007) Further, voltage-gated $Na^+$-channels ($Na_V$) enable fast electrical signalling in the RPE (Johansson et al., 2019), while both $Na_V$ and voltage-gated $Ca^{2+}$ -channels ($Ca_V$) have been shown to be involved in the POS phagocytosis, one of the prime functions of the RPE (Johansson et al., 2019; Korkka et al., 2018).

Gap junctions regulate the overall electrical properties of the RPE in cooperation with the ion channels and transporters by allowing the free transfer of small ions and molecules between the adjacent RPE cells. Gap junctions are intercellular channels composed of two juxtaposed hemichannels, hexameric structures formed of six connexin proteins. (Sosinsky and Nicholson, 2005) The primary connexin protein expressed in vertebrate RPE is Connexin 43 (Cx43) (Janssen-Bienhold et al., 1998). Another, more weakly expressed connexin type present in the RPE is Connexin 36 (Cx36) (Fadjukov et

al., 2022). In addition, gap junctions modulate the phagocytic activity of the tissue (Fadjukov et al., 2022; Zielicka et al., 2015).

### 2.4.2 Photoreceptor outer segment phagocytosis

Photoreceptor cells, rods and cones, consist of four components: an outer segment, an inner segment, a cilium connecting the outer and inner segments, and a synaptic terminal. The POS in rods are built from individual discs, while in cones the outer segments are invaginations connected to the plasma membrane. (Kevany and Palczewski, 2010) The outer segments contain opsins, G protein-coupled receptors associated with a chromophore such as rhodopsin in the case of rods (Terakita, 2005).

When the entering light reaches the photoreceptors, it is absorbed fully in the outer segments by opsins, which then initiate the visual transduction pathway. Over time, continuous exposure to light generates photo-oxidative damage in the outer segments. To limit the damage caused, the POS are continuously replaced by synthesizing new, fresh discs at the base of the photoreceptors, while simultaneously shedding the old, damaged discs at the tip of the outer segments. (Kwon and Freeman, 2020) 7 to 10 % of the entire POS mass is removed every two weeks resulting in a high turnover (Kevany and Palczewski, 2010). RPE is responsible for mediating the turnover of the discs, with each cell being connected to approximately 30 photoreceptor cells (Young and Bok, 1969).

The microvilli of the RPE begin to probe and eventually ensheathe the outer segments of the photoreceptors to be shed. (Kwon and Freeman, 2020) Proper ensheathment of the POS requires the apically targeted receptor tyrosine kinase MERTK. MERTK stimulates the activation of factors required for the branching of fibrous actin, which forms a structure called the phagocytic cup around the POS. (Almedawar et al., 2020; Kwon and Freeman, 2020) The formed structures, phagosomes, are 1-2 μm in size and undergo a complex maturation process. The resulting drop in the pH of the phagosomes results in the enzymatic breakdown of their content (Kwon and Freeman, 2020) Most of the POS mass is made of glycosylated opsin, while the rest is mostly polyunsaturated lipids, which results in the need for activated proteases, glycosidases and lipases to ensure proper digestion (Goldberg et al., 2016). The formed solutes are released from the phagosomes, and parts of the POS components are recycled back to the photoreceptors as building blocks for fresh discs. Incomplete POS breakdown leads to the accumulation of lipo- and melanolipofuscin, both a mix of oxidized proteins and lipids, eventually leading to retinal disorders. (Kennedy et al., 1995)

### 2.4.3 Light absorption and shielding from photo-oxidation

The pigmented structure of the RPE assists in absorbing scattered light and improving spatial resolution. The entering light leaves the RPE and the whole retina suspectable for oxidative damage, which the RPE combats with the melanosomes and antioxidants. (Strauss, 2005)

Melanosomes are lysosome-related organelles, where the pigment molecule melanin is synthesized (Barral and Seabra, 2004). The dark colour reflects the melanin pigment's ability to absorb and dissipate almost all frequencies of visible light making it effective at shielding the RPE and the retina from photo-oxidative stress (Solano, 2014). The melanosomes are located in the apical cytoplasm of the RPE and have been shown to change their distribution with the light cycle. A momentary threefold increase in the number of melanosomes in the regions surrounding the photoreceptors has been recorded after light onset. (Barral and Seabra, 2004) Additional support for light absorption is offered by the photoreceptors, which contain carotenoids focused on the absorption of blue light (Strauss, 2005). Blue light is especially dangerous to the RPE due to its photo-oxidative effect on the lipofuscin granules formed during POS-phagocytosis leading to the formation of toxic substances (Boulton et al., 2004). In addition to its light-absorptive properties, the melanosomes act as antioxidants by neutralizing the harmful reactive oxygen radicals alongside other antioxidants present in the RPE, including superoxide dismutase, carotenoids, and β-carotene. (Strauss, 2005)

### 2.4.4 The visual cycle

When the entering light reaches the photoreceptors, it is absorbed by the opsins, G protein-coupled receptors with a chromophore such as retinal connected to them. (Terakita, 2005). When light is absorbed by rhodopsin, the opsin found in rods, its chromophore 11-*cis*-retinal undergoes isomerization to all-*trans*-retinal. The all-*trans*-retinal is rapidly released from the opsin and enzymatically reduced to all-*trans*-retinol, allowing opsin to bind a new chromophore for continuous light absorption. (Rando, 2001) The formed all-*trans*-retinol is transported to the RPE with the assistance of IRBP (Rando, 2001) and peropsin, a non-visual opsin localized in the photoreceptor-surrounding microvilli of the RPE (Cook et al., 2013; Sun et al., 1997).

In the RPE, the all-*trans*-retinol is esterified by the acyl transferase (LRAT) at the smooth endoplasmic reticulum of the RPE (Kiser et al., 2014; MacDonald and Ong, 1988), before the retinoid isomerohydrolase retinal pigment epithelium 65 kDa protein (RPE65) catalyses the conversion of all-*trans*-retinol to 11-*cis*-retinol (Kiser, 2022; Moiseyev et al.,

2005). Finally, the 11-*cis*-retinol is oxidized back into 11-*cis*-retinal by 11-*cis*-retinol dehydrogenase in a reaction supported by the cellular retinaldehyde-binding protein (CRALBP), which localizes in the microvilli. The 11-*cis*-retinal is then transported out of the RPE back to the photoreceptors mediated by IRBP. (Kiser et al., 2014; Rando, 2001) In addition to the cycle described above, an alternative visual cycle pathway used by the cone cells exists, where Müller glia are utilized instead of the RPE (Mata et al., 2002; Wang and Kefalov, 2011).

## 2.5 Retinal pigment epithelium-related diseases

The role of the RPE in the maintenance of the neural retina is vital, which is highlighted by the arising issues in the case of RPE dysfunction. Two common examples include AMD and RP. AMD is the leading cause of blindness in people over the age of 60 in the developed world, with over 200 million patients worldwide (Wong et al., 2014). The disease can be divided into “dry” and “wet” forms, from which dry AMD is the most common form in the early stage, and wet in the more advanced stages of the disease. The dry form is characterized by the presence of lipid deposits, drusen, in the macula. In wet AMD, neovascularization occurs in the macula causing fluid leakage into the retina. (C. J. Thomas et al., 2021) RPE degeneration is often seen in patients with AMD. The number of RPE cells reduces alongside detected depigmentation and changes in cell morphology, as well as increased lipofuscin concentration. (Feldman et al., 2022; Somasundaran et al., 2020) Complete treatment options for the dry form are currently nonexistent, but in certain cases, it is possible to slow down the progression of the disease. For wet AMD, photodynamic therapy and anti-VEGF factors are used with limited success. (C. J. Thomas et al., 2021) New treatment possibilities are studied continuously, with e.g. retinal organoids in the spotlight (B. B. Thomas et al., 2021).

RP is a heterogeneous inherited retinal disease highlighted by the progressive loss of photoreceptors (Hartong et al., 2006). Over a million patients have been recorded worldwide (Fahim, 2018). For example, mutations in the *RPE65* -gene causing dysfunction of the RPE65-dependent visual cycle have been linked to RP. (Morimura et al., 1998) Treatment options for RP are more established compared to AMD with gene therapy treatments, including the FDA-approved Luxturna, been shown to be somewhat viable (Prado et al., 2020). Gene therapy methods are often verified using organoid models (Belova et al., 2022; Völkner et al., 2021). Therefore, the investigation of new and improved gene therapy treatments goes well hand-in-hand with the research of improved RPE and RO models (Fahim, 2018).

## 2.6 Stem cells

Stem cells are unspecialized cells with the ability for self-renewal. Depending on their developmental potency, stem cells can differentiate into various cell types. Totipotent stem cells, such as the zygote, can differentiate into any cells allowing them to form whole organisms. Pluripotent stem cells, such as embryonic stem cells, can form all germ layers of an embryo. Multipotent stem cells are able to specialize in distinct cells of specific lineages, for example, the different blood cells as in the case of hematopoietic stem cells. Oligopotent stem cells can divide into a more limited set of cell types, while unipotent stem cells are only able to self-renew. (Zakrzewski et al., 2019)

Human pluripotent stem cells, mainly human embryonic (hESCs) and human induced pluripotent stem cells (hiPSCs) are often used in research. Human embryonic stem cells are derived from the early human embryo, and using various culturing protocols (for example, Alsanie et al., 2013; Erceg et al., 2008) differentiated into the cell types of interest. (Pera et al., 2000) iPSCs are reprogrammed from differentiated cells such as fibroblasts. By using already differentiated cells, iPSCs offer the possibility to create extremely specific pluripotent cell lines from, for example, the patient's own cells. (Takahashi et al., 2007) One of the main issues with iPSCs is the low efficacy of the method as typically less than 1 % of transfected fibroblasts undergo reprogramming (Yamanaka, 2012). Both hESC and iPSC-derived RPE have been generated and are commonly utilized (for example, Hazim et al., 2017; Johansson et al., 2019). The various RPE models, including the well-established pluripotent models used in research, are discussed in more detail next.

## 2.7 Retinal pigment epithelium models

### 2.7.1 Two-dimensional RPE cell cultures

The two-dimensional RPE cell cultures can be divided into three main groups: primary cell cultures, stem cell-derived cultures, and RPE cell lines. Primary RPE cultures from human fetal tissue (Blenkinsop et al., 2013; Mannagh et al., 1973), or harvested from rodent (Gibbs and Williams, 2003), porcine (Toops et al., 2014) or bovine eyes generally form coherent, polarized and functional RPE monolayers. Well-polarized RPE can be detected after four (Maminishkis et al., 2006) and two weeks (Toops et al., 2014) in primary cultures derived from human and porcine sources, respectively. The lack of access to available tissues is one of the main issues related to primary cultures. In addition, the ethical and practical concerns around using human fetal and non-human tissue need to

be considered. Restrictions on NIH funding for human fetal tissue-related research were made fairly recently limiting the usage of human fetal RPE (MacDuffie et al., 2021). While porcine and bovine primary cultures are well-established, the existence of human-specific genes and resulting diseases sets certain limitations to using non-human tissues (Lakkaraju et al., 2020).

Differentiated RPE cell lines have been developed and utilized for years, but the initial cell lines suffered from challenges regarding the morphology and polarity of the cells (Nabi et al., 1993; Rambhatla et al., 2002). Recent advances in the adult RPE-19 (ARPE-19) cell line have enabled the common use of RPE cell lines in research. However, the RPE characteristics of the cell line seem to have diminished during the years (Lakkaraju et al., 2020) in addition to the polarity of the tissue varying based on the culturing conditions (Bonilha, 2014; Luo et al., 2006), and the cell line expressing all tight junction proteins except claudins (Peng et al., 2016). Despite the issues, the cell line continues to be widely used in RPE research.

Stem cell-derived cultures refer to cultures differentiated from either induced pluripotent or embryonic stem cells. Stem cell-derived human RPE forms mature cultures in approximately 10-12 weeks of culturing (Johansson et al., 2019; Viheriälä et al., 2022). Generally, stem cell-derived RPE is well-established and routinely used in various research (Johansson et al., 2019; Korkka et al., 2018) due to the existence of many efficient published protocols (for example, Hazim et al., 2017).

The current golden-standard for 2D RPE is the RPE monolayer cultured on transwell cell culture inserts (Lynn et al., 2018; Sonoda et al., 2009; Viheriälä et al., 2022). Cell culture inserts can be classified as a type of scaffold since the porous membrane of the insert mimics the features of the underlying Bruch's membrane. The presence of the membrane enables the RPE to fulfil some of its *in vivo* functions, including directional epithelial transport, which can result in a highly polar RPE monolayer. (Lynn et al., 2018) However, the varying protocols between different laboratories result in high variation in the RPE and results achieved with the scaffold method in addition to the other challenges related to 2D RPE.

Overall, the two-dimensional RPE cell culture models are functional and display both morphology and polarity somewhat similar to native RPE, especially when cultured on inserts. As mentioned in the context of RPE maturation, the RPE and the photoreceptors require support from one another during the development process. The absence of a neural retina and the IPM in the cell cultures results in limited cell-matrix interactions of

the RPE followed by altered tissue function, and thus limited capacity for disease modelling (Oswald and Baranov, 2018). For example, the direct comparison between 2D and 3D hESC-derived RPE showed the lack of adherence junctions, desmosomes, and basal caveolae in the 2D tissue, all of which were present in the 3D RPE. Transcriptome analysis confirmed that between the two cultures, the 3D culture had the highest correlation with native RPE. (Wu et al., 2016) More advanced cell culture models are required for achieving RPE that resembles the *in vivo* tissue more closely.

### 2.7.2 Ex vivo and tissue-engineered models

One option for obtaining samples that resemble the native RPE is to use native tissue itself. Flatmounts from prepared animal RPE with or without the surrounding tissues offer one of the best opportunities to study *in vivo* RPE. (Lakkaraju et al., 2020) They have been used in e.g., RPE live imaging and histological experiments with success (Lakkaraju et al., 2020; Zhang et al., 2019). If prepared with the surrounding tissues intact, flatmounts offer the possibility to study the function of the RPE in almost its natural environment. However, in addition to the challenging procedure and limited availability of tissue, flatmounts are short-lived maintaining their characteristics for only some hours in culturing media (Lakkaraju et al., 2020).

Scaffolds are structures acting as temporary support for the implanted cells by e.g., promoting cell adhesion and growth in addition to acting as physical support (Chen et al., 2002). Scaffold-based tissue-engineered RPE and retina offer possibilities for retinal tissue repair and pre-clinical models (Tan et al., 2018). For example, porous, fibrous and hydrogel-based scaffolds for RPE have been developed. In all mentioned cases, the scaffold morphology is created to mimic that of Bruch's membrane to enable efficient RPE adhesion, proliferation and differentiation. Since scaffolds are built as temporary structures, they are replaced by the ECM produced by the RPE cells themselves resulting in an *in vivo* -like environment. (Liu et al., 2021; Tan et al., 2018) Despite the promising possibilities, scaffold-based RPE cultures are not yet in common use due to difficulties in manufacturing, with low cell affinity, toxic scaffold degradation products, and complicated protocols being common issues (Liu et al., 2021)

Similarly to scaffold-based approaches, 3D bioprinting offers opportunities for establishing RPE cell cultures closer to *in vivo* RPE than 2D cultures. Various materials including alginate, hyaluronic acid and Matrigel have been used as the basis for the hydrogel bioinks used in bioprinting (Selcan Gungor-Ozkerim et al., 2018). Multilayer bioprinting approaches have been utilized with RPE and neural retina with moderate success (Masaeli et al., 2020; Masaeli and Marquette, 2020; Song et al., 2023; Wang et al., 2018). In the

experiments by Wang et al. (2018), the focus was on the improved maturation of the photoreceptors in the presence of RPE. The maturation of the RPE itself was not considered in the article. In the experiments by Masaeli and Marquette (2020), low cell viability was reported across all cell types, including the RPE. Song et al. (2023) engineered a bioprinted 3D outer retina barrier structure with an established RPE monolayer on top. Using the model, they were able to reveal an RPE-dependent choroidal phenotype in AMD. Another multilayer experiment by Masaeli et al. (2020) included a three-layer bioprinted structure with a Bruch's membrane-mimicking Gelatin Methacrylate layer, an ARPE-19 layer, and a photoreceptor layer with photoreceptors isolated from adult pig ocular globes. Throughout the one-week experiment, all layers proliferated, and high cell viability was reported. However, the one-week timeline is not feasible for estimating the benefits of the structure for the maturation of the RPE. All of the examples above highlight the increasing potential of bioprinted approaches. More research is required before making further assumptions on the effects of the bioprinted structures on the maturation of the RPE.

### 2.7.3 Retinal organoids

Stem cell-derived three-dimensional cultures mimicking the original organ structures, organoids, offer the opportunity to study tissues in an *in vivo* -like environment (Lancaster and Knoblich, 2014). Retinal organoids (ROs) have been used for the study of the retina for over a decade (Eiraku et al., 2011). Various RO protocols derived from both hESCs and iPSCs have been developed over the years with the organoids containing multiple retinal cell types and attaining functionality. In addition, the samples are not short-lived as in the case of flatmounts. (Zhang et al., 2021; Zhong et al., 2014)

The main approaches to generating ROs can be divided into 3D, and a combination of 2D and 3D techniques, which are separated by the embryonic body (EB) -phase. In the 3D technique, the EBs are generated in the beginning, with the optic vesicle and optic cup phases following suit (Nakano et al., 2012). In the 2D-3D combinatory technique, the EB-phase is bypassed and instead, optic vesicles are generated directly (Zhong et al., 2014). In addition to the two main approaches, the generation of ROs can be modified by adding various supplements, such as FGF or RA to the cultures to e.g. accelerate the maturation of the photoreceptors (Brooks et al., 2019; Zerti et al., 2020).

In the RO cultures, the focus is often on the improved maturation of the photoreceptors instead of the RPE. Indeed, one of the common issues with ROs is the absence of RPE from the organoids, or its presence as separate patches instead of structures in close cooperation with the neural retina (Cowan et al., 2020; Isla-Magrané et al., 2021). There

have been attempts to counter the issue with co-cultures. For example, the RPE-photoreceptor interphase has been attained with the generated ROs being co-cultured with 2D RPE cultures (Akhtar et al., 2019), but once again the focus has been on the photoreceptors. Furthermore, the culturing protocols for ROs are often expensive and laborious, with culturing times of up to hundreds of days with regular manual detaching of the developing structures (Regent et al., 2020). To harness the potential of organoids as models for e.g., retinal diseases, less challenging and less time-consuming protocols are required in addition to attaining proper RPE structure.

## 2.8 Optic vesicle containing-brain organoids

In 2021, Gabriel et al. published a protocol for human brain organoids with forebrain-like regions that spontaneously assemble functional bilateral optic vesicles. The OVB-organoids constitute the cellular components of a developing optic vesicle, including primitive corneal epithelial and lens-like cells, RPCs, RPE, axon-like projections and electrically active neuronal networks with e.g. myelinated cortical neurons and microglia (Gabriel et al., 2021). Opposed to the ROs discussed before, the OVB-organoids do not contain mature photoreceptors. Instead, the presence of intrinsically photosensitive retinal ganglion cells (ipRGCs) was detected, which explains the reported light sensitivity of the organoids. (Gabriel et al., 2021) The presence of RPE as a properly positioned monolayer together in close connection with the neural retina could have positive effects on the maturation of the RPE even without the presence of the matured photoreceptors.

# 3. AIMS OF THE THESIS

Various retinal diseases can be traced back to the dysfunction of the RPE. The continuous research of treatment options for mentioned diseases requires improved RPE cell models, which better mimic the *in vivo* tissue in morphology and function. One possibility is the further development of organoid models. In 2021, Gabriel et al. published a protocol for OVB-organoids with the pigmented optic vesicles of the organoids containing RPE. This thesis aimed to differentiate OVB-organoids from the hESC cell line Regea 08/017 to be used as a model for RPE maturation. The three main aims of the study were as follows:

1) To differentiate viable OVB-organoids that produce optic vesicles by the 60-day timepoint.
2) To characterize the contents of the developed optic vesicles and confirm the presence of RPE. The characterization was done with gene expression analysis and cryosectioning of the optic vesicles followed by immunofluorescence stainings.
3) To assess the maturity of the RPE in the optic vesicles. The maturity was assessed based on the gene expression and immunofluorescence staining results from the characterization after the presence of RPE was confirmed.

# 4. MATERIALS AND METHODS

## 4.1 hESC culturing

In the article (Gabriel et al., 2021), the OVB-organoids were derived from iPSCs. In this thesis, the organoids were derived from the hESC line Regea 08/017 (Skottman, 2010), a commonly used hESC line in the Skottman and Nymark laboratories. Initially, the cells were cultured on laminin 521 (LN521) (Biolamina, Sweden) coated well plates in Essential 8 (E8) (Thermo Fisher Scientific, United States) cell culture medium, which is a commonly used culturing method for hESCs in the Skottman laboratory. (Hongisto et al., 2017). Due to limited success in the organoid formation, the culturing method was changed to Matrigel (Corning, United States) coated well plates in mTeSR1 (STEMCELL™ Technologies, Canada) cell culture medium as described by Gabriel et al. (2021). The cells were cultured at +37°C in 5 % $CO_2$ with regular medium changes.

## 4.2 OVB-organoid culturing

The OVB-organoid culturing includes three distinct phases as described by Gabriel et al. (2021). The three phases were identical for all of the organoids, regardless of the hESC culturing method. The first phase, neural induction, lasted five days during which the hESCs committed to their neural fate and formed a neurosphere at the bottom of each 96-well plate well. In the second phase called the neurosphere phase, the neurospheres formed at the end of the neural induction were cultured further before being moved on to the third and final phase, the organoid phase. In the organoid phase, the neurospheres developed and matured into OVB-organoids, which were cultured for up to 60 days. The OVB-organoids were collected for characterization on days 20, 50 and 60 of the organoid phase. The culturing and characterization process is summarised below in Figure 4. The figure describes the length and characteristics of the three phases in addition to the characterization methods chosen for the early- (days 20-25 of the organoid phase) and late-phase (days 50-60 of the organoid phase) organoids.

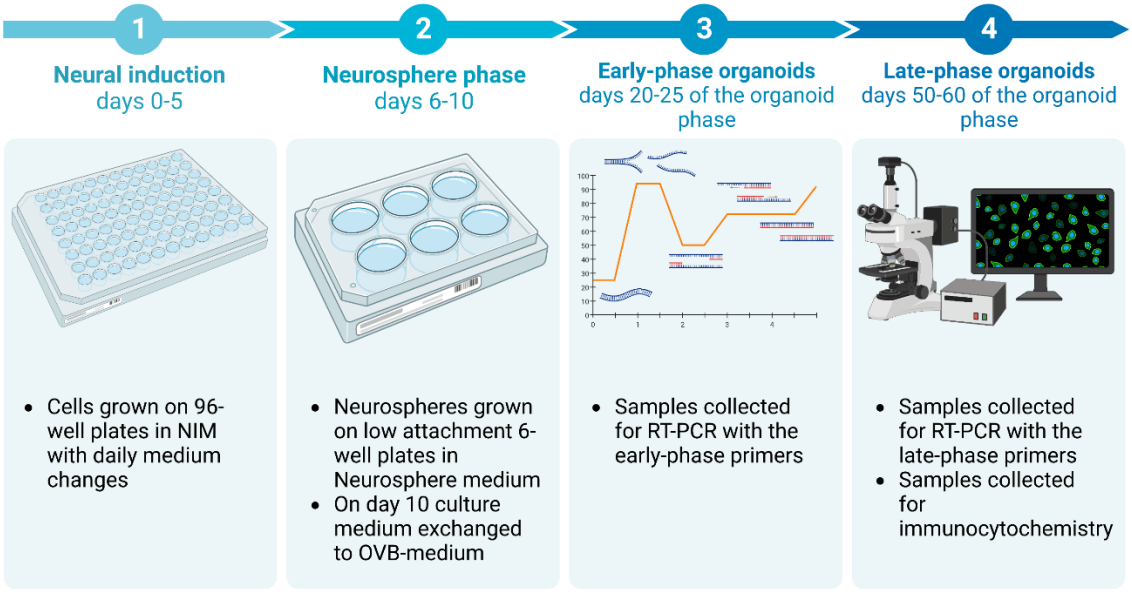


***Figure 4**. A summary of the culturing and characterization process of the organoids. Created with BioRender.com*

### 4.2.1 Neural induction

The hESCs cultured on either LN521- or Matrigel-coated plates were dissociated into single cells. The hESC plates were washed with 1X PBS before incubating with TrypLE™ Select (Thermo Fisher Scientific) for 3-4 minutes at +37°C. After incubation, TrypLE™ Select was removed and Defined Trypsin Inhibitor (DTI) (Thermo Fisher Scientific) was used to detach and collect the cells for counting with a Bürker counting chamber. $1x10^6$ cells were diluted in 10 ml of Neural Induction Medium (NIM) (STEMCELL™ Technologies) with 10 μM Y-27632 (ROCK-inhibitor) (Selleck Chemicals, United States).

96-well Polystyrene Conical Bottom MicroWell plates (Thermo Fisher Scientific) were coated with 80 μl of Anti-Adherence rinsing solution (STEMCELL™ Technologies). After aspiration, the well plates were rinsed with warm 1X PBS. The PBS was aspirated from the wells and 100 μl of the cell solution was added to each well. The cells were incubated at +37°C in 5 % $CO_2$. Half of the NIM was refreshed daily for five days until neurosphere formation. The organoids were imaged daily during neural induction with Nikon Eclipse TE2000-S Inverted microscope (Nikon, Japan).

### 4.2.2 Neurosphere phase

The formed neurospheres were collected after day 5 of neural induction with a cut 100 μl pipette tip and moved to Corning Costar® Ultra-Low Attachment 6-well plates (Merck,

Germany) in Neurosphere medium (Supplemental Table 1). The neurospheres were incubated at +37°C in 5 % $CO_2$ for five days. On the third day 500 µl of OVB-medium (Supplemental Table 2) was added to each well. The organoids were imaged during the neurosphere phase with Nikon Eclipse TE2000-S Inverted microscope (Nikon).

### 4.2.3 Organoid phase

On the fifth day of the neurosphere phase, the neurospheres were either collected and moved to spinner flasks (Corning) containing 100 ml of the OVB culturing medium (Supplemental Table 2), or the neurosphere medium was aspirated from the wells and replaced with OVB medium. The organoids were cultured at +37°C in 5 % $CO_2$ for up to 60 days with medium changes once per week until day 25 of the organoid phase, and twice per week after. The organoids were imaged during the organoid phase with either Leica DMi8 Inverted (Leica Microsystems, Germany), Nikon Eclipse TE2000-S Inverted (Nikon) or Nikon Eclipse FN1 Upright microscope (Nikon). The images were adjusted with linear brightness and contrast adjustments with Fiji (Schindelin et al., 2012). The size of the organoids and eventually their optic vesicles were measured with Fiji. Three diameter measurements from the angles 0°, -90° and -45° were taken from each sample, and their average was calculated.

## 4.3 Characterization

### 4.3.1 Gene expression analysis

RNA was isolated from 20-, 50- and 60-days old organoids. For the 50 and 60-day-old organoids samples, mainly organoids without visible pigmented vesicles were collected to ensure enough samples for immunocytochemistry experiments. The organoids were collected, washed with 1X PBS, and centrifuged into pellets. RNeasy Mini kit (Qiagen, Netherlands) was used for the RNA isolation. The RNA concentrations were measured with the NanoDrop™ 2000 spectrophotometer (Thermo Fisher Scientific). The isolated RNA was diluted to 20 ng/µl for the cDNA reverse transcription with the High-Capacity cDNA Reverse Transcription Kit (Applied Biosystems, Unites States).

For the gene expression analysis, RT-PCR with either the AccuPrime™ Taq (Invitrogen, United States) or the DreamTaq™ (Thermo Fisher Scientific) DNA Polymerase kit. The sequences for the early- and late-phase primers can be found in Supplemental Table 3 and 4, respectively.

### 4.3.2 Immunocytochemistry

60-day-old late-phase organoids with visible pigmented vesicles were collected, washed with PBS-Glycine (0.225 g Glycine per 100 ml 1X PBS), and fixed in 4 % PFA for 30 min at room temperature (RT). The organoids were dehydrated in a 30 % sucrose solution at +4°C overnight. The following day the organoids were embedded into Tissue-Tek O.C.T.™ Compound (Sakura Finetek, The Netherlands) and stored at -80°C. Frozen samples were cryosectioned at 12 µm thickness with the Cryostat MEV+ (SLEE medical GmbH, Germany) and placed onto Epredia™ Superfrost™ Plus Adhesion microscope slides (Thermo Fisher Scientific). The slides were incubated for 1 hour at RT before storing at +4°C overnight or directly moving to the antibody stainings.

Before the stainings, the microscope slides were incubated for 30 min at RT if they had been stored at +4°C overnight. The samples were washed 2 x 3 min with PBS-Glycine and permeabilized with 0.5 % Triton-X-100/0.1 % Tween-20 (Sigma-Aldrich, United States) in 1X PBS -solution for 15 min at RT. After another 2 x 3 min wash with PBS-Glycine, the samples were blocked with 3 % BSA-PBS solution for 1 h at RT. The primary antibodies, which can be found in Supplemental Table 5, were diluted in the blocking solution and incubated for 2 h at RT. After 3 x 3 min washing with the blocking solution, the secondary antibodies (goat anti-Mouse Alexa 488, goat anti-Rabbit Alexa 568, and phalloidin) (Thermo Fisher Scientific) were diluted 1:200 in the blocking solution and incubated for 1 h at RT in the dark. Finally, the samples were incubated with DAPI for 5 minutes at RT in the dark, followed by brief air-drying and mounting with ProLong Diamond Antifade (Invitrogen) and glass coverslips. Slides were air-dried for a minimum of 1 hour before storing at +4°C.

The samples were imaged with Zeiss LSM 800 laser confocal microscope (Carl Zeiss, Germany) and the Zeiss Plan-Apochromat 63x/1.40, WD 0.19 oil objective (Carl Zeiss). Maximum intensity projections from the images were created with Fiji (Schindelin et al., 2012). All channels were adjusted with linear brightness and contrast adjustments.

# 5. RESULTS

## 5.1 hESC culturing

Initially, the organoids were differentiated from hESCs cultured on LN521 coated plates in E8 cell culture medium, which is the commonly used culturing method for hESCs in the Skottman laboratory. Later, the hESC culturing method was exchanged for the Matrigel-mTeSR1 -method, as described in the materials and methods. Both culturing methods produced hESCs suitable for organoid differentiation but the differences between the methods resulted in differences in the quality of the organoids, as discussed later.

## 5.2 OVB-organoid culturing

Initiation of the neural induction was successful regardless of the hESC culturing method. The differences in the hESC culturing method became apparent in the neurosphere and especially the organoid phase when the organoids derived from hESCs cultured on LN521 began adhering to their environment and each other. The adherence issue prompted the switch to the Matrigel-mTeSR1 hESC culturing method, as described in the original article by Gabriel et al. (2021). In the organoid phase, the organoids were initially transferred to spinner flasks for further culturing. The spinner flasks were left out from further attempts due to unexpected issues with their function (see section 5.2.3), and the organoids were kept on ultra-low attachment well plates throughout the organoid phase instead.

From now on, the organoids derived from hESCs cultured on LN521 or Matrigel coated plates will be referred to in the text as LN521- or Matrigel-organoids, respectively. The neural induction, neurosphere, and organoid phases were identical for both the LN521- and Matrigel-organoids.

### 5.2.1 Neural induction

The neural induction of the organoids was successful with both LN521- (Figure 5) and Matrigel-organoids (Figure 6). 96 EBs (here referred to as neurospheres as in the original article) from hESCs cultured on LN521 coated plates and 192 neurospheres from hESCs cultured on Matrigel coated plates were differentiated for this thesis work. In both culturing methods, the hESCs produced round neurospheres with clear borders, as seen in

Figures 5 and 6. The Matrigel-hESCs produce initially smaller neurospheres, which grew in size during neural induction to match the size of the LN521-hESC neurospheres.

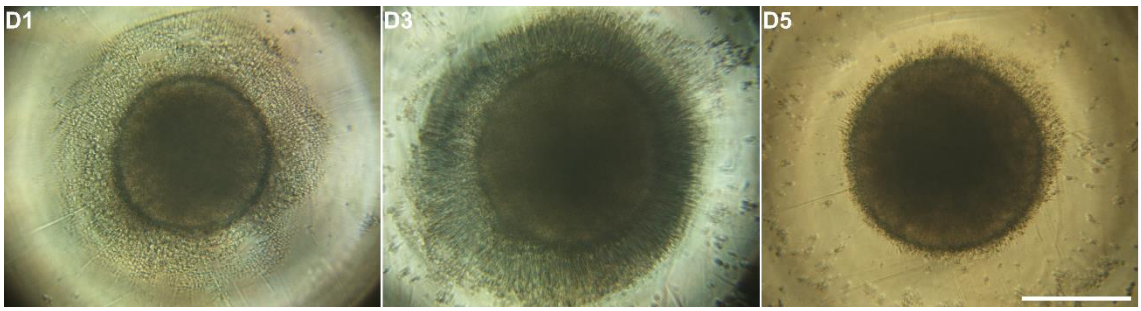


***Figure 5**. The neural induction phase of LN521-organoids. Images were taken on days 1, 3 and 5 of the neural induction. Scale bar 500 µm. Imaged with Nikon Eclipse TE2000-S 4x objective.*

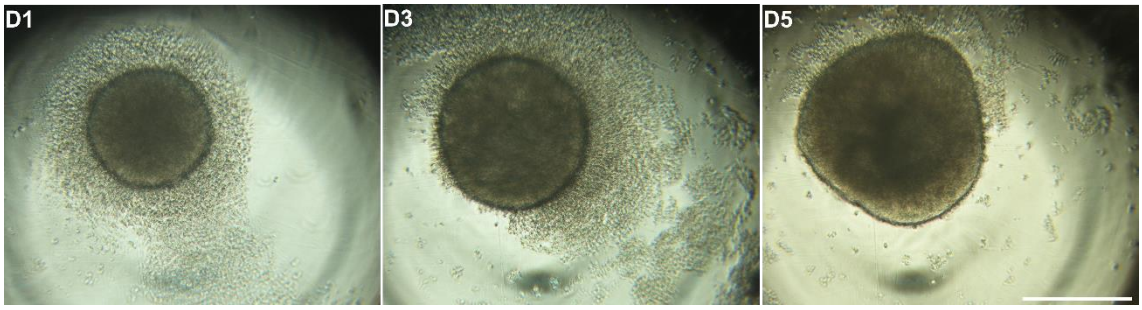


***Figure 6**. The neural induction phase of the Matrigel-organoids. Images were taken on days 1, 3 and 5 of the neural induction. Scale bar 500 µm. Imaged with Nikon Eclipse TE2000-S 4x objective.*

### 5.2.2 Neurosphere phase

The differences between the hESC culturing methods became apparent in the neurosphere phase. Compared to the LN521-organoids (Figures 7 A and B), the Matrigel-organoids (Figures 7 C and D) held their shape and structure better in the neurosphere phase. The LN521-organoids more often either broke down or formed complexes by adhering to each other. After three days of the neurosphere phase, the surviving individual LN521-organoids seemed to be slightly smaller in size compared to the Matrigel-organoids.

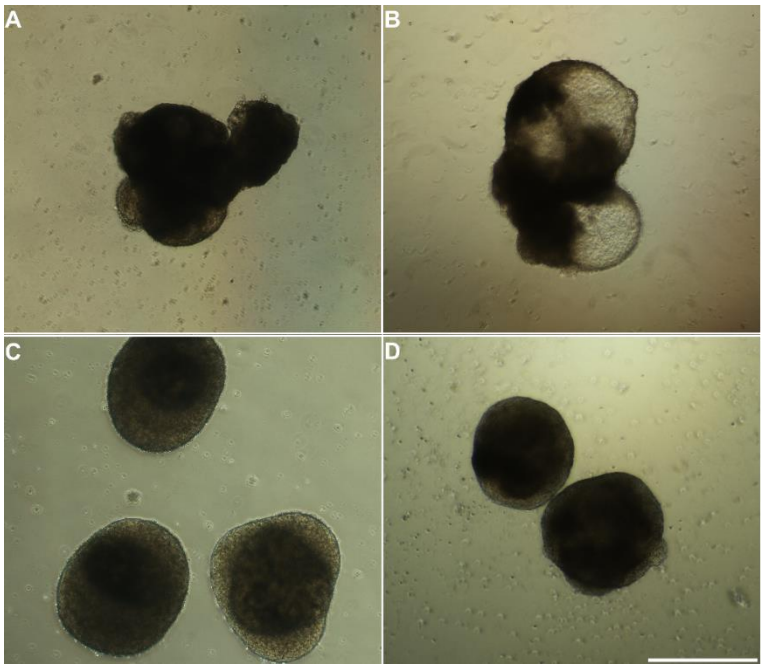


***Figure 7**. Day three of the neurosphere phase of the organoids. The images show broken down or adhered LN521-organoids (A) and (B), and individual and healthy Matrigel-organoids (C) and (D). Scale bar 500 µm. Imaged with the Nikon Eclipse TE2000-S 4x objective.*

The number and percentage of produced neurospheres that survived the five-day neurosphere phase to the beginning of the organoid phase are presented in Table 1. For both the LN521- and Matrigel-organoids the survival percentage was 84.4 %.

***Table 1.** The number and percentage of both LN521- and Matrigel-organoids that survived from the neural induction phase to the beginning of the organoid phase.*

| Organoids | n (d5 neural induction) | n (d0 organoid phase) | Percentage (%) |
|---|---|---|---|
| LN521 | 96 | 81 | 84.4 |
| Matrigel | 192 | 162 | 84.4 |

### 5.2.3 Organoid phase

Initially, about half of the LN521-organoids (n = 39) were moved to the spinner flasks for the duration of the organoid phase. The rest of them (n = 42) were left to grow on the ultra-low attachment well plates with the idea of comparing the effects of the spinner flask and the well plate on the morphology of the developing organoids and their vesicles. The LN521-organoids were heavily adhering to the sides and blades of the spinner flasks resulting in the loss of most of the organoids during the first 2-3 weeks of the organoid phase. The remaining few (n = 6) were moved back to the ultra-low attachment well plates.

Due to the adherence issue, the culturing method of the hESCs was exchanged for the Matrigel-mTeSR1-based method, which was the chosen method for the iPSCs in the original article (Gabriel et al., 2021). The initial tests with the Matrigel-organoids showed, that they adhered to the spinner flasks with less frequency compared to the LN521-organoids. The initial test results are not otherwise reported in this thesis. However, the single-use spinner flasks did not seem to survive the several rounds of washing and disinfecting between attempts resulting in a weakened function of the blades. Due to the continuation of the adherence issue combined with the noticeably weakened spinner flask function, further organoid cultures were conducted only on the ultra-low adherence well plates.

The number and percentage of the neurospheres from the neural induction that developed into OVB-organoids with at least one optic vesicle (see Figures 9 and 10) by day 60 of the organoid phase are provided in Table 2. 6.25 % of the LN521- and 4.69 % of the Matrigel-organoids had developed at least one vesicle.

***Table 2**. The percentage of neurospheres that developed into OVB-organoids with at least one optic vesicle by day 60 of the organoid phase.*

| Organoids | n (d5 neural induction) | n with vesicles (d50 + d60) | Percentage (%) |
|---|---|---|---|
| LN521 | 96 | 6 | 6.25 |
| Matrigel | 192 | 11 | 5.73 |

The developing Matrigel-organoids were imaged and measured approximately once a week. The diameters of the Matrigel-organoid bodies from each of the timepoints can be seen in Figure 8 A. The number of organoids imaged in each timepoint varied due to the limitations of the imaging setup since the organoids could not be returned to the cell culture after imaging. On timepoints, where organoids were collected for further experiments (days 20, 50 and 60), more samples could be imaged. The number of imaged Matrigel-organoids and the median measurements in each timepoint are listed in Table 3 below.

***Table 3.*** *The number of imaged organoids and the median values of the diameters in each timepoint of the Matrigel-organoid body measurements.*

| Timepoint (d) | Number of organoids | Median measurement (µm) |
|---|---|---|
| 0 | 1 | 454.2 |
| 7 | 3 | 304.9 |
| 14 | 1 | 319.9 |
| 20 | 7 | 878.7 |
| 28 | 1 | 730.3 |
| 35 | 1 | 766.3 |
| 50 | 24 | 644.0 |
| 60 | 18 | 1182.2 |

As seen in Figure 8 A, the measured diameters of the organoid bodies vary noticeably between the samples at each timepoint. The diameters of the optic vesicles (n = 9) in the 60-day-old Matrigel-organoids can be seen in Figure 8 B. The median value for the vesicle measurements was 221.7 µm with vesicle diameters ranging from 128 µm to 290 µm.

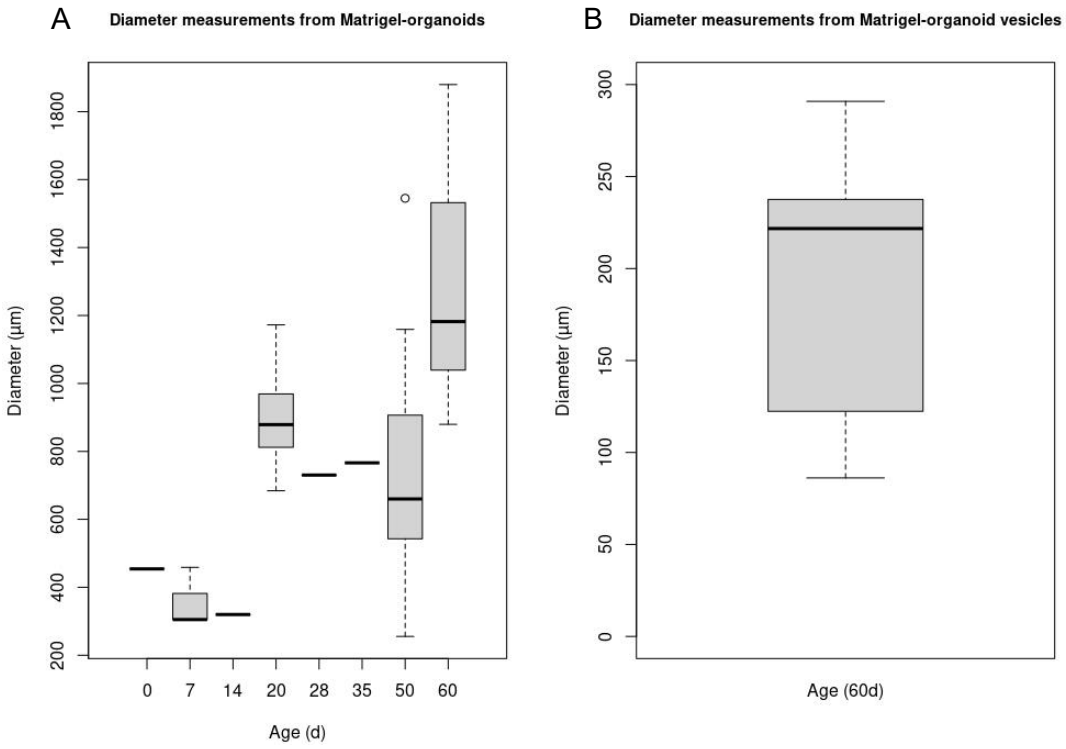


***Figure 8****. Diameter measurements from Matrigel-organoids bodies (A) and the developed vesicles (B). For (B), n = 9 pigmented vesicles.*

Examples of LN521- and Matrigel-organoids are shown in Figures 9 and 10, respectively. The Matrigel-organoids held their compact shape better, while the LN521-organoids

grew relatively large loose extensions of the main body. Regarding size, there seem to be no noticeable differences between the main body sizes of the organoids.

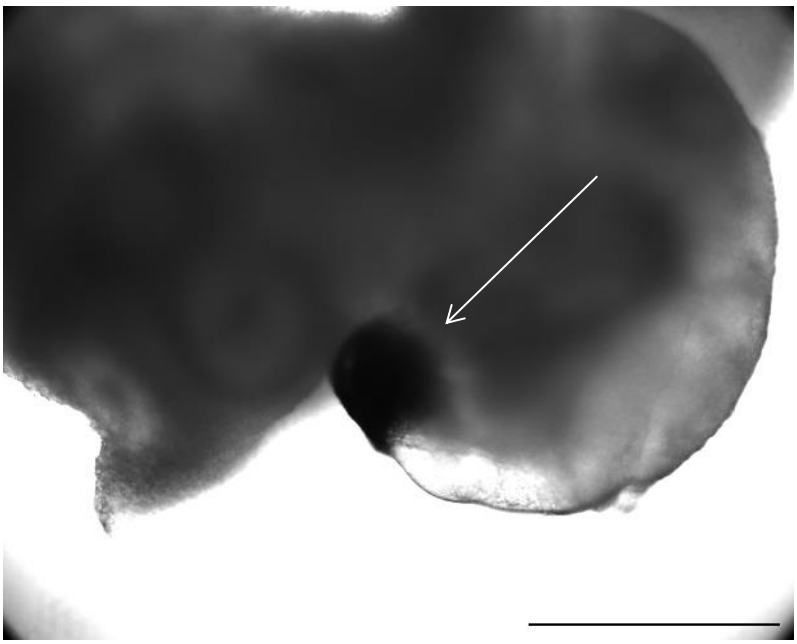

***Figure 9**. A 60-day-old late-phase LN521-organoid. The optic vesicle has been marked with an arrow. Scale bar 500 µm. Imaged with the Nikon Eclipse FN1 Nikon Plan Fluor 10x/0.3 air objective.*

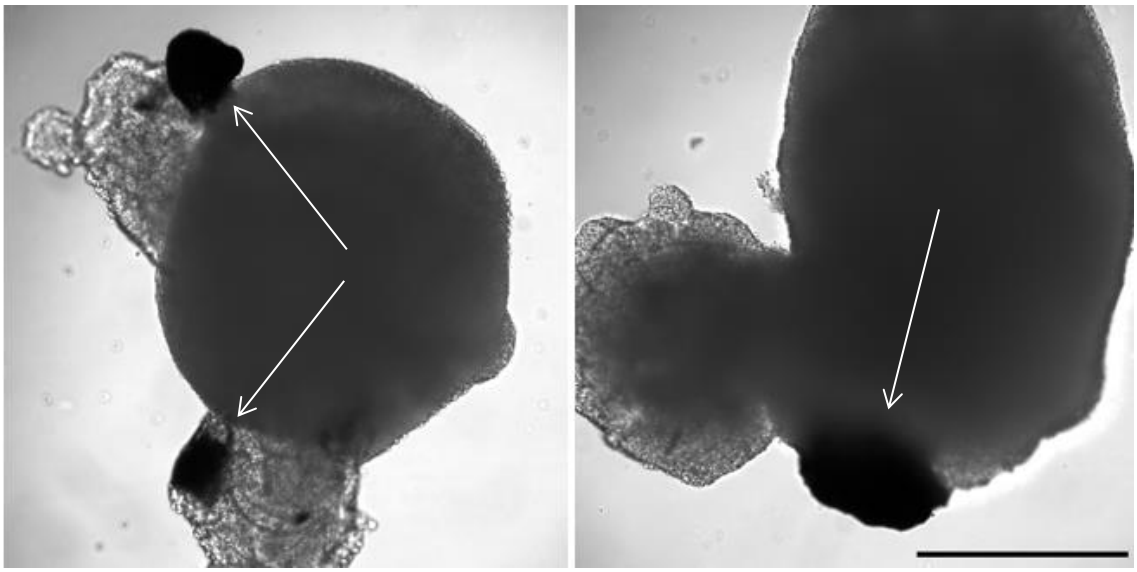

***Figure 10**. 60-day-old late-phase Matrigel-organoids. Two optic vesicles can be seen in the organoid on the left, and one in the organoid on the right. The vesicles have been marked with arrows. Scale bar 500 µm. Imaged with the Leica DMi8 10x objective.*

## 5.3 Gene expression analysis

Early- and late-phase organoids were collected on days 20 and 60 of the organoid phase for gene expression analyses conducted with RT-PCR, as described in the summary in Figure 4. Additionally, RT-PCR was conducted for 50-day timepoint Matrigel-organoids, the results of which are shown in Supplemental Figure 1.

### 5.3.1 Early-phase organoids

The results from the early-phase PCR for both LN521- and Matrigel-organoids are shown in Figure 11. For the Matrigel-organoids, two additional primers *OTX2* and *SOX2* were chosen. Expression of *PAX6* and *GAPDH* are seen in both samples, while expression of *RAX* can only be seen in the LN521-organoid sample. *POU5F1* (Oct3/4) is not expressed in either sample. The expression of *OTX2* is seen in the Matrigel-organoid sample, while the results for *SOX2* seem to correlate with something expressed in the water control sample.

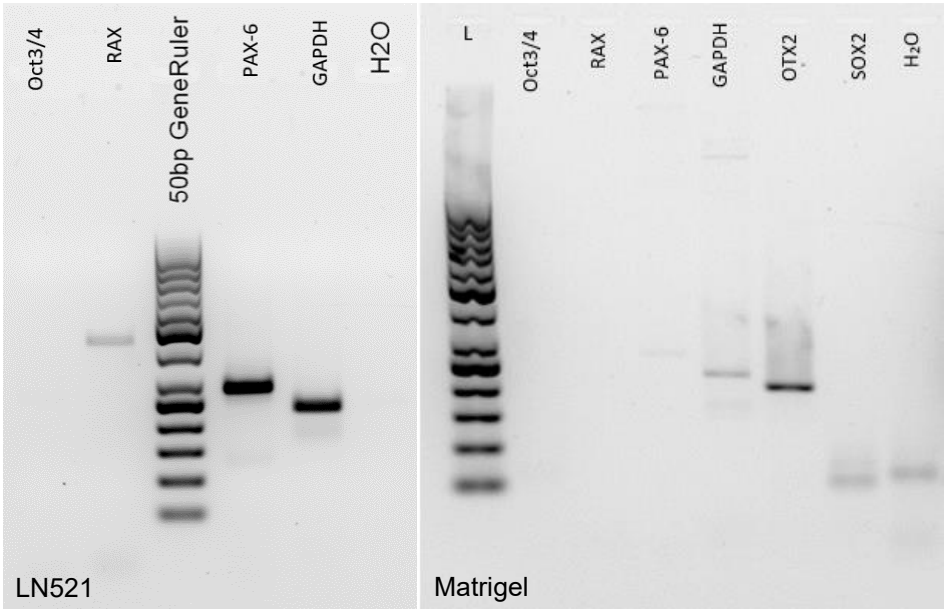


***Figure 11**. 20-day-old early-phase LN521- (on the left) and Matrigel-organoids (on the right). Both samples are from one batch of LN521- or Matrigel-organoids. L = GeneRuler 50 bp DNA ladder (Thermo Fisher Scientific), $H_2O$ = water control.*

### 5.3.2 Late-phase organoids

The results of the late-phase organoid RT-PCR are shown below in Figure 12. The expression for *MITF*, *MERTK*, *CALB2* and *GAP43* is seen in both LN521- and Matrigel-organoid samples. *GJA1* (Cx43) is expressed only in the LN521-organoid and not in the

Matrigel samples, while the opposite is true for *RPE65*. No expression of *GAD2*, *RCVRN* (Recoverin), *CLDN19* (CL-19) or *RRH* (peropsin) can be seen in either sample. As Figure 12 shows, something expressed in the water control sample seems to be present in almost every other sample as well.

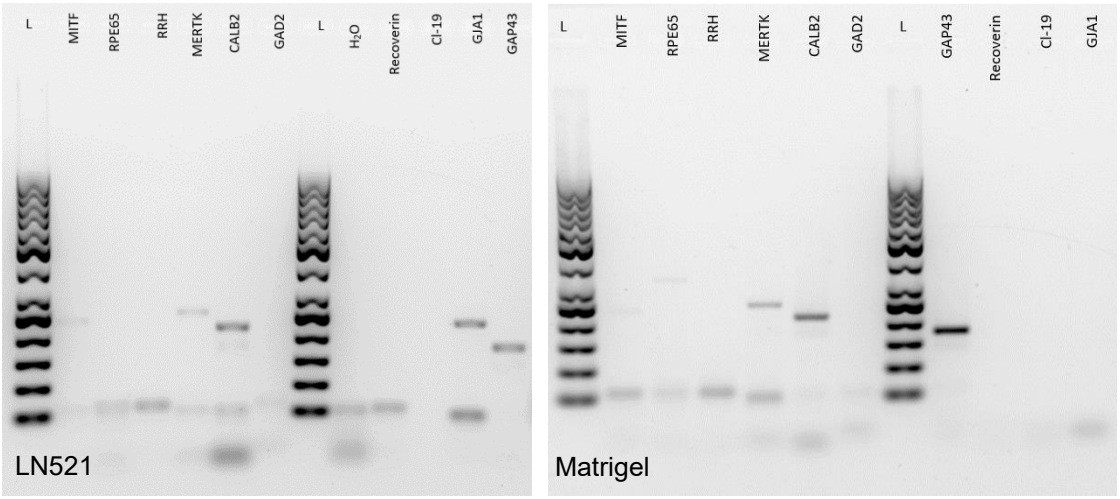


***Figure 12**. 60-day-old late-phase LN521- (on the left) and Matrigel-organoids (on the right). Both samples are from one batch of LN521- or Matrigel-organoids. L = GeneRuler 50 bp ladder (Thermo Fisher Scientific). $H_2O$ = water control.*

In Table 4, the expression of genes detected in the LN521- and Matrigel-organoids by RT-PCR is compared to the RNA-sequencing and gene enrichment analyses presented by Gabriel et al. (2021). Four of the genes analyzed and presented by Gabriel et al. (2021) are expressed in the LN521-organoids and five in the Matrigel-organoids. *POU5F1, MITF*, *Cl-19*, *CLDN19*, *GJA1*, *RRH* and *MERTK* were not considered in the original article and are novel results from this thesis work.

***Table 4.*** *Comparison between the gene expression analysis results of the LN521- and Matrigel-organoids, and the RNA sequencing results presented by Gabriel et al. (2021). The markings indicate the specific gene was either expressed (+) or not expressed (-) in the samples, or no data was available (nd).*

| Gene | LN521-organoids | Matrigel-organoids | Gabriel et al. |
|---|---|---|---|
| *POU5F1* (Oct3/4) | - | - | nd |
| *PAX6* | + | + | + |
| *Rax* | + | - | + |
| *OTX2* | nd | + | + |
| *SOX2* | nd | - | + |
| *CALB2* | + | + | + |
| *GAP43* | + | + | + |
| *RPE65* | - | + | + |
| *GAD2* | - | - | + |
| *RCVRN* (Recoverin) | - | - | + |
| *MITF* | + | + | nd |
| *MERTK* | + | + | nd |
| *GJA1* (Cx43) | + | - | nd |
| *CLDN19* (Cl-19) | - | - | nd |
| *RRH* (peropsin) | - | - | nd |

## 5.4 Protein localization analysis

Results of the immunofluorescence stainings of the 60-day-old Matrigel-organoids can be found in Figures 13 and 14. For comparison, immunofluorescence stainings of 8-week-old hESC-RPE cultured on cell culture inserts are presented in Supplemental Figures 2, 3 and 4. In Figure 13 in each panel, the first image (T-PMT) is a brightfield image of the stained cryosection showing the pigmented areas assumed to contain RPE. The second image shows channel 488 nm, which was used to stain different structures of interest. The channel 568 nm used to stain the actin cytoskeleton with phalloidin is shown in the third image, and the cell nuclei stained with DAPI in the fourth. The fifth image shows the merged image of all channels except T-PMT.

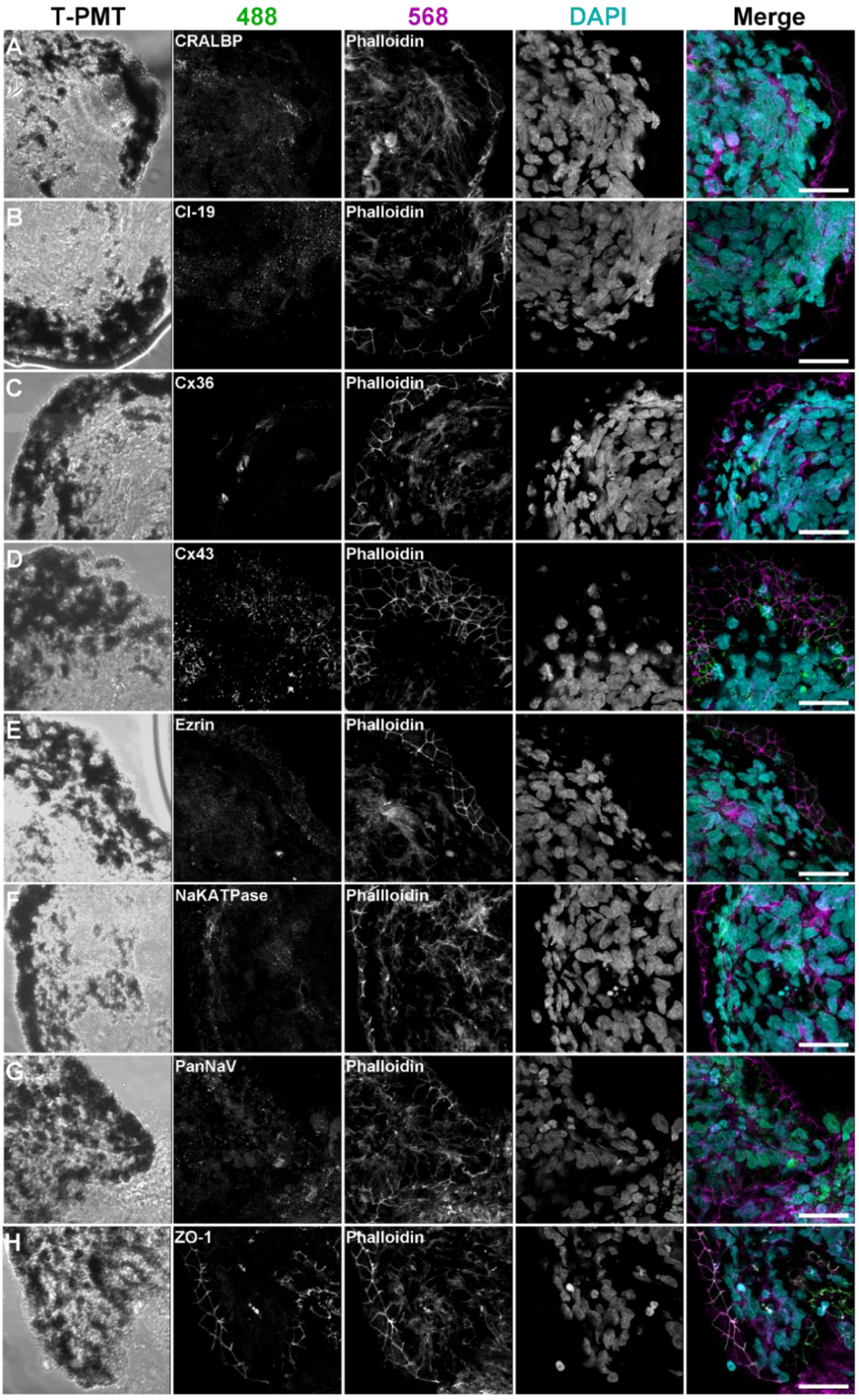
T-PMT
488
568
DAPI
Merge
A
CRALBP
Phalloidin
B
Cl-19
Phalloidin
C
Cx36
Phalloidin
D
Cx43
Phalloidin
E
Ezrin
Phalloidin
F
NaKATPase
Phalloidin
G
PanNaV
Phalloidin
H
ZO-1
Phalloidin

***Figure 13**. Immunofluorescence stainings of the 60-day-old late-phase Matrigel-organoid cryosections. Scale bar 20 µm. Imaged with the Zeiss Plan-Apochromat 63x/1.40 oil objective. In each panel (A-H), the first image (T-PMT) is a brightfield image showing the pigmented areas expected to contain RPE. The third image (568) shows the channel 586 nm used to stain the actin cytoskeleton of each cryosection with phalloidin. The fourth image (DAPI) shows the nuclei of the cells as stained by DAPI, and the fifth image (Merge) is the merged image of all the channels except T-PMT. The second image (488) shows the channel 488 nm, which was used to stain different structures: CRABLP (A), Cl-19 (B), Cx36 (C), Cx43 (D), Ezrin (E), Na/K-ATPase (F), PanNa$_V$ (G) and ZO-1 (H).*

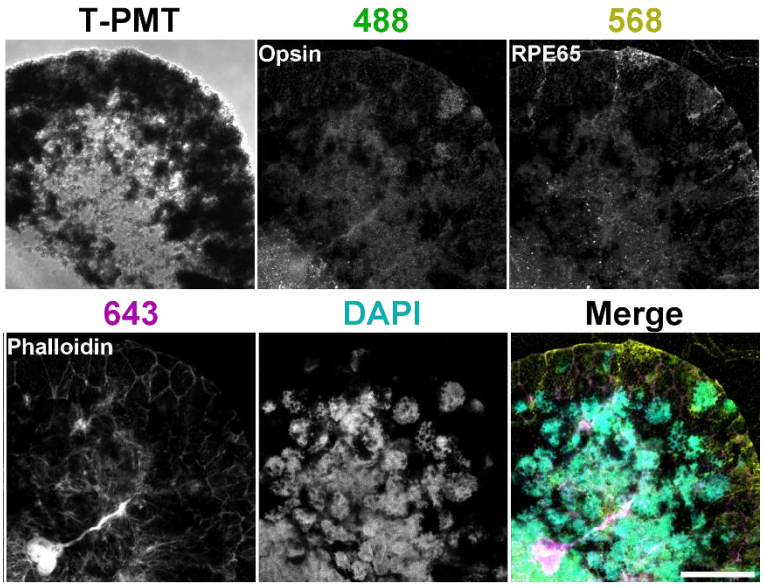


***Figure 14**. Immunofluorescence stainings of the late-phase organoid cryosections. The first image on top (T-PMT) is a brightfield image showing the pigmented areas of the cryosection expected to contain RPE. The second (488) and third (568) images on top show the channels 488 nm and 568 nm, which were used to stain opsin and RPE65, respectively. The first image on the bottom (643) shows the channel 643nm used to stain the actin cytoskeleton of the cryosection with phalloidin. The second image on the bottom (DAPI) shows the nuclei of the cells as stained by DAPI, and the final image (Merge) is the merged image of all the channels except T-PMT. Scale bar 20 µm. Imaged with the Zeiss Plan-Apochromat 63x/1.40 oil objective.*

In both Figures 13 and 14, the honeycomb-like hexagonal structure of the RPE can be detected in each sample as stained by phalloidin, a toxin used to stain the actin cytoskeleton. In Figure 13 A, CRALBP can be seen to somewhat localize inside the suspected RPE cells. A noticeable amount of CRALBP is also seen in the areas lacking pigment. Cx36 and Cx43 are shown in Figures 13 C and D, respectively. In Figure 13 C, Cx36 localizes in areas mostly outside of the pigmented area detected in the brightfield image, while Cx43 is seen to localize with the honeycomb structures stained by actin, as well as the pigmented areas seen in the brightfield image. Similar localization is seen for ezrin,

a linker between the plasma membrane and the actin cytoskeleton, (Figure 13 E) and ZO-1, a TJ protein (Figure 13 H). Na/K-ATPase and $PanNa_V$ seem to localize in the suspected RPE cells as seen in Figures 13 F and G. Na/K-ATPase localizes slightly more inside the individual cells while following the cell borders, while $PanNa_V$ localizes more evenly in the tissue.

In Figure 14, RPE65 is localized in the suspected RPE, with some individual stained spots seen in the unpigmented areas. Opsin on the other hand can be seen to mainly localize outside the pigmented areas, again with some individual stained areas in the pigmented area. The opsin seen in the pigmented areas seems to somewhat correlate with the localization of RPE65.

# 6. DISCUSSION

## 6.1 OVB-organoid culturing

The initial organoids were derived from hESCs cultured on LN521-coated plates in E8 cell culture medium. In the organoid phase, the LN521-organoids were heavily adhering to the sides and blades of the spinner flask in addition to forming larger complexes by adhering to each other. Due to the issue, the hESC culturing was instead done on Matrigel-coated plates in mTeSR1 cell culture medium, as described in the original article by Gabriel et al. (2021). The change reduced the adherence issue in the organoid-phase and resulted in larger, more durable organoid structures.

According to the manufacturer Corning, Matrigel is “a solubilized basement membrane preparation extracted from the Engelbreth-Holm-Swarm mouse sarcoma” (https://www.corning.com/worldwide/en/products/life-sciences/products/surfaces/matrigel-matrix.html, 20.3.2023). Due to Matrigel being derived from an animal source, it has a noticeable batch-to-batch variability in addition to its’ specific composition being unknown. The batch-to-batch variability is one of the reasons why the LN521-E8 -culturing method is the preferred method for hESCs in the Skottman laboratory. The primary components of Matrigel are the four basement membrane proteins: laminin (c. 60 %), collagen IV (c. 30 %), entactin (c. 8 %), and heparin sulphate proteoglycan perlecan (c. 2-3 %) (Aisenbrey and Murphy, 2020). The predominant laminin in Matrigel has been identified as laminin 111, which contains multiple binding sites for various cell types and is known to promote differentiation (Aisenbrey and Murphy, 2020; Timpl et al., 1979). Because of its origin, Matrigel contains several tumour-derived proteins including various growth factors and enzymes (Aisenbrey and Murphy, 2020). All of the mentioned factors could have affected the differentiation and maturation of the Matrigel-organoids, resulting in them having formed more durable and vigorous structures with less adherence to their surroundings. In addition, since Matrigel was present in the Neurosphere medium (Supplemental Table 1) of the neurosphere phase, the Matrigel-based hESC culturing method could have offered a more continuous organoid differentiation path since the cells used were familiarized with Matrigel.

Both E8 and mTeSR1 are widely used media for feeder-free cell cultures. E8 is a chemically defined media (Chen et al., 2011), while mTeSR1 contains animal-sourced components such as BSA (Ludwig et al., 2006). According to the manufacturer STEMCELL™ Technologies, all raw components of the mTeSR1 are pre-screened to ensure batch-to-

batch similarity (https://www.stemcell.com/products/mtesr1.html, 9.4.2023). The pre-screening methods are not discussed further, which makes it challenging to estimate the true batch-to-batch variability of the animal components. The most likely assumption would be that each batch has slight variations but fulfils the requirements set by the manufacturer. In studies, mTeSR1-Matrigel culturing conditions are more often credited for producing better results regarding pluripotent stem cell differentiation (Hey et al., 2018), while E8-Vitronectin culturing conditions result in less variation between the differentiation state of the cells (Cornacchia et al., 2019; Jeong et al., 2020). Conversely, many studies state how the culturing medium had no significant effects on the results of the differentiation, and the results are credited to the coating substance or other factors (Lei et al., 2014; Patel and Alahmad, 2016; Prakash Bangalore et al., 2017). Based on the literature, the effect of the coating substance seems to be more significant compared to the effect of the culturing media. To test the effect of specifically the hESC culturing media on the derived organoids, the hESC culturing should be conducted on the same coating substance in the chosen media.

As seen from Table 1, the percentage of organoids that survived from the neural induction and through the neurosphere phase finally to the beginning of the organoid phase was 84.4 % for both LN521- and Matrigel-organoids. Some singular neurospheres were lost when collected and moved from the 96-well plate to the ultra-low adhesion 6-well plates at the end of neural induction and the beginning of the neurosphere phase. During the neurosphere phase, most of the occurring neurosphere loss happened during the addition of the OVB-medium (Supplemental Table 2) during the third day of the neurosphere phase, regardless of the coating used during the hESC culturing.

The difference between the Neurosphere (Supplemental Table 1) and the OVB (Supplemental Table 2) culturing media was the addition of dorsomorphin and B-27 supplement with retinyl acetate (RA), the natural form of vitamin A, to the OVB medium. Dorsomorphin is a bone morphogenetic protein (BMP) and AMP-activated protein kinase (AMPK) pathway inhibitor, which suppresses mesoderm, endoderm and trophectoderm differentiation while inducing neural conversion (Zhou et al., 2010). Combined with SB431542, an inhibitor of the Activin/BMP/TGF-β pathway present in both the Neurosphere and OVB culturing media, dorsomorphin promotes efficient neural induction and the differentiation of neural progenitor cells from pluripotent stem cells (James et al., 2005; Morizane et al., 2011)

RA on the other hand is vital for embryonic eye development due to its role in promoting the development of the ventral retina and the optic nerve and inhibiting the mesenchyme around the optic cup (Cvekl and Wang, 2009). RA acts as a type of signalling switch from

the proliferating pluripotent stem cells to the differentiation of neuronal cells and eventually the optic vesicle (Cvekl and Wang, 2009; Janesick et al., 2015). Since both dorsomorphin and RA promote the switch from the pluripotent phase to neural conversion, they could have acted as a so-called quality control step for the organoids in the neurosphere phase. The neurospheres that broke down after the addition of the OVB medium could be the ones that were not able to make the switch to differentiation. Interestingly, there was no difference between the LN521- and Matrigel-organoids concerning the survival percentages indicating a more built-in rather than culture condition-related response to the addition of the OVB medium.

The percentage of neurospheres from the neural induction that developed into OVB-organoids with at least one optic vesicle by day 60 of the organoid phase was 6.25 % for LN521- and 5.73 % for Matrigel-organoids as listed in Table 2. In the original article, the yield of OVB-organoids for the iPS cell line IMR-90 was 17.9 % with 86 organoids out of five batches containing at least one optic vesicle (Gabriel et al., 2021). IMR-90 was the chosen cell line in the article used for further characterization and experiments. Compared to 17.9 %, the below 7 % yield from the hESCs is low. The difference could be attributed to cell line variation. In the original article, the total yield of OVB-organoids differed noticeably between the iPSC lines. For the cell lines GM25256 and Crx-iPS, the yields were 37.7 % and 33.3 % with 182 organoids out of four, or 96 organoids out of three batches, respectively (Gabriel et al., 2021). Further optimization of the OVB protocol for hESCs could help improve the yield since differences between e.g., gene expression levels and differentiation properties of iPSCs and hESCs have been reported before (Narsinh et al., 2011). Some optimization of the original protocol was done already during this thesis work regarding the organoid-phase. Instead of the organoids being cultured in the spinner flasks as in the original article (Gabriel et al., 2021), the culturing was optimized to be done on ultra-low adherence well plates instead. The difference in the yields between the LN521- and Matrigel-organoids (Table 2) was most likely due to the aforementioned properties of the LN521- and Matrigel-culturing methods. In addition, more Matrigel-organoids were collected during the experiments for, for example, imaging and RNA extractions leaving fewer samples for the day 60 timepoint.

Organoids were collected for further experiments on days 20 and 60. In addition, Matrigel-organoids mainly without noticeable vesicles were collected for RNA extraction on day 50 to ensure enough samples for the immunocytochemistry experiments on day 60. As listed in Table 3, the median size of the Matrigel-organoids collected on day 50 was 644 µm, and on day 60 1182.2 µm. The number of Matrigel-organoids with optic vesicles collected on day 50 was two (n = 2) and on day 60 nine (n = 9). Based on the data in

Table 3 and Figure 8 A, the size of the Matrigel-organoid bodies that develop vesicles were larger compared to the ones that do not. As a comparison, while the exact sizes of the 60-day-old organoids presented in the original article were not reported, from the figures provided they could be estimated to have a body diameter of 2-3 mm (Gabriel et al., 2021). The difference in the sizes of the organoid bodies between the iPSC-derived organoids of the original article and the hESC -derived organoids reported in this thesis could be dependent on the need for further optimization of the protocol for hESCs. The differences could also be the result of cell line variation.

In Figure 8 B, the median diameter of the 60-day-old Matrigel-organoid vesicles was 221.7. In the original article, the precise sizes were not reported but the organoids could be estimated to have vesicles with a diameter of about 200 – 400 µm. Once again, the difference in sizes could be dependent on the cell line variation or the need for further optimization of the protocol.

## 6.2 Gene expression analysis

Organoids were collected for gene expression analyses on days 20 and 60. In addition, Matrigel-organoids were collected on day 50 as well. The results of the 20-day-old early-phase gene expression analyses can be seen in Figure 11. Since *POU5F1* (Oct3/4) is a marker gene for the pluripotent phase, it was not expressed in the organoids marking the success of the differentiation, as expected. In the LN521-organoid sample, both *RAX* (409 bp) and *PAX6* (274 bp) were visible and located in the correct positions indicating the expression of the early eye genes. *GAPDH* (229 bp) is a housekeeping gene used as a positive control. The *GAPDH* band for LN521-organoids was the correct size and dark indicating a sufficient concentration of cDNA present in the samples.

In the Matrigel-organoid sample, expression of *PAX6* was detected, but in a lower quantity compared to the LN521-sample. No expression of *RAX* was seen in the Matrigel-organoid sample. *PAX6* is the master gene for eye development, while *RAX* is an early-eye gene required for retinal cell fate (Sadler and Langman, 2012; Slavotinek, 2011). In the original article (Gabriel et al., 2021), *PAX6* was used specifically as an eye field patterning and *RAX* as an early retina development marker. Based on this, the LN521- and Matrigel-organoids both expressed the gene required for the formation of the eye field and the development of the eyes, but only the LN521-organoids expressed the gene crucial for further retinal development. However as discussed later, both the late-phase LN521- and Matrigel-organoids expressed retinal genes. The reason for *RAX* not being expressed in the early-phase Matrigel-organoids could be that the 20-day timepoint is still too early for them. In addition, the expression of *GAPDH* was noticeably lower in the

Matrigel- than in the LN521-organoid sample. The low cDNA concentration could mean that the possible expression of *RAX* in the Matrigel-organoids was simply not detected.

For the early-phase Matrigel-organoids, two additional genes *OTX2* and *SOX2* were included in the gene expression analysis. *OTX2*, a downstream product of *TGF-β*, drives the differentiation of the RPE from the outer layer of the optic cup. *SOX2* is the regulatory target of *PAX6* and as such is involved in the establishment of the eye field in early eye development. (Sadler and Langman, 2012) Based on Figure 11, *OTX2* (200 bp) was expressed in the Matrigel-organoids, while *SOX2* (155 bp) was not. The band located in the *SOX2* sample was not the correct size, and based on the water control sample was most likely the result of primer dimers or other impurities. Since *PAX6* expression in the Matrigel-organoid sample was notably low, the expression of *SOX2* may have been too low to be detected at the time. The early-phase Matrigel-organoid RT-PCR should be conducted again with a more concentrated cDNA sample to be certain of the results.

The results of the 60-day-old late-phase LN521- and Matrigel-organoid gene expression analyses can be found in Figure 12. *MITF* (225 bp), *RPE65* (324 bp), *RRH* (379 bp), *MERTK* (250 bp)*, GJA1* (300 bp) and *CLDN19* (151 bp) are genes expressed in the RPE as discussed in the literature review. *CALB2* (215 bp) and *GAD2* (140 bp) are expressed in horizontal and amacrine cells and *GAP43* (167 bp) in retinal ganglion cells. *RCVRN* (120 bp) is detected primarily in retinal cells, specifically in the photoreceptors.

The lack of or low expression of RPE-related genes such as *RRH* and *CLDN19,* or *RPE65* and *MITF*, respectively, in the LN521- and Matrigel-organoids could mean that even though there was RPE present in the pigmented optic vesicles, it was not yet mature. To check the maturation level of the RPE in the organoids, further functionality and morphology tests could be conducted on RPE extracted from the organoids. In the case of the Matrigel-organoids, mainly samples without the pigmented vesicles were chosen for the 60-day timepoint gene expression analysis to ensure enough material for the immunofluorescence staining experiments. Since the dark pigment in the optic vesicles is expected to originate from the RPE, it would be sensible that organoids without visible pigmented vesicles would not express RPE-related genes. However, all available LN521-organoids at the 60-day timepoint, including six organoids with optic vesicles, were used for the late-phase gene expression analysis. The results from the LN521-organoids support the idea of the not yet matured RPE.

The absence of *RCVRN*, the gene encoding the protein Recoverin, was expected since in the original article the OVB-organoids were not reported to express mature photoreceptors (Gabriel et al., 2021). *CALB2* and *GAD2* are both markers for amacrine and

horizontal cells used in the original article. Out of the two, *GAD2* is expressed more in horizontal cells. Therefore, the lack of its expression in both samples implies the lack of horizontal cells in the organoids.

All of the extra bands seen in both samples in Figure 12 were from small products (> 50 bp), which would indicate either primer dimers or individual primers. The actual RT-PCR products were over 150 bp long, making the interpretation of the results possible, however, the late-phase PCR should be conducted again to be sure. In addition, more samples with pigmented vesicles should be chosen for the RNA extractions to attain more reliable results on the gene expression of the vesicles. Redoing the PCR experiments was unfortunately not possible in the time scale of the thesis project.

Table 4 summarises the gene expression analysis results of the LN521- and Matrigel-organoids to the RNA sequencing results presented in the original article (Gabriel et al., 2021). The results indicate that the organoids differentiated in this thesis were not identical to the OVB-organoids produced in the original article. It is possible, that the optimization of the culturing protocol, and repetition of the gene expression analyses with more OVB-organoids with optic vesicles could improve the results. Six of the analysed genes, *POU5F1, MITF*, *MERTK*, *GJA1*, *CLDN19* and *RRH*, were considered for the first time in this thesis work. Five out of six mentioned genes (all but *POU5F1*) are either related to the direct development of the RPE or expressed in the RPE (Janssen-Bienhold et al., 1998; Kwon and Freeman, 2020; Otani and Furuse, 2020; Sadler and Langman, 2012; Sun et al., 1997).

## 6.3 Protein localization analysis

The results of the protein localization analysis are presented in Figures 13 and 14. The hexagonal structure of the RPE is especially clear in Figure 13 D, where the pattern correlates well with the pigmented areas seen in the brightfield (T-PMT) image. For comparison, immunofluorescence stainings of 8-week-old hESC-RPE cultured on cell culture inserts are shown in Supplemental Figures 2, 3 and 4, where the same hexagonal pattern can be seen more clearly. Both ezrin (Figure 13 E) and ZO-1 (Figure 13 H) are seen to localize with the actin cytoskeleton strongly indicating the presence of RPE in the samples.

The connexins, in Figured 13 C and D, should both be located in the gap junctions in the RPE cell membranes. Cx43 is highly expressed and localizes in the cell borders, while the expression of Cx36 in the sample is low. Cx43 is the main type of connexin found in the RPE, while Cx36 is expressed more weakly in the tissue (Fadjukov et al., 2022;

Janssen-Bienhold et al., 1998), which explains the observed differences in their expression.

In Supplemental Figure 2, CRALBP localized inside the RPE cells. The same can be seen in Figure 13 A, merely on a smaller scale. Na/K-ATPase and PanNa$_V$ in Figures 13 F and G, respectively, localize in the suspected RPE cells. In RPE inserts, Na/K-ATPase (Supplemental Figure 3) localizes as individual dots in the RPE cells and the cell borders. PanNa$_V$, used to stain the Na$_V$ ion channels, (Supplemental Figure 4) localizes equally everywhere in the cells with less regard for cell borders. Similar behaviours can be seen in the Matrigel-organoid samples. RPE65 in Figure 14 is localized in the RPE, while opsin is not. RPE65 is localized in the RPE, while opsin enters the RPE during POS phagocytosis when the outer segments of the photoreceptors are engulfed by the RPE cells.

Based on the immunofluorescence staining results, especially the localization of RPE65, Cx43 and ezrin combined with the hexagonal honeycomb structures revealed by phalloidin and ZO-1, the pigmented vesicles contain RPE in the outer layer of the optic vesicles. In the original article by Gabriel et al. (2021), the focus was on the photoreceptors. RPE or its maturation were not discussed in any detail making the comparison of the thesis results to the original publication challenging.

## 6.4 Future directions

As of the writing of this thesis, the original article by Gabriel et. al. (2021) has been cited 32 times according to the Web of Science, usually as an example of recent progress in the field of retinal and brain organoids. Compared to retinal organoid protocols, the OVB-organoid protocol is rather simple, which would make it a noteworthy option for the production of laborious ROs. However, the repeatability of the protocol could be the limiting factor and the reason why no repeated results have been published in a year and a half. Despite numerous previous attempts not reported in this thesis, we were not able to culture the organoids in the spinner flasks, and our yield of organoids with optic vesicles was extremely low. The failures could be explained by the differences between cell lines or the usage of hESCs instead of iPSCs. Even in the results reported in the original article, the yield of optic vesicles varied greatly between different iPS cell lines. The main step of optimization in the original article was finding the optimal concentration of RA. By readjusting the RA concentration for the hESC-derived organoids, the yield could be improved. In addition, by attempting to differentiate the organoids from the iPS cell lines utilized in the original article, the repeatability of the protocol could be properly tested.

Another reason for the lack of repeated results in any publication since 2021 could be the overall focus on photoreceptors in the RO field of study. The OVB-organoids lacked mature photoreceptors, which are often the focus of interest when designing and developing ROs (Cowan et al., 2020; Isla-Magrané et al., 2021). Even if the OVB-organoids are not a suitable model for studying photoreceptor maturation, the presence of the neural retina component could improve the maturation of the RPE making them a viable option in RPE research.

In future experiments, the maturity of the RPE in the OVB-organoids should be properly assessed. By extracting the RPE grown in the organoids and culturing it further on cell culture inserts, the functionality and morphology of the RPE could be investigated with immunofluorescence stainings, TEER-measurements, $Ca^{2+}$-imaging, and POS-phagocytosis, all commonly used methods in assessing RPE maturity. Even with additional research required to make further assumptions on the maturity or functionality of the RPE in the OVB-organoids, this thesis has succeeded in its original goal of differentiating the OVB-organoids and verifying the RPE and its state of maturation within. The OVB-organoids offer a new and interesting possibility for culturing mature RPE to be used in both basic research and research aimed at improved treatment options for various retinal diseases.

# 7. CONCLUSIONS

The differentiation of OVB-organoids from the Regea 08/017 cell line was successful. Based on the late-phase gene expression and protein localization analysis results, the pigmented optic vesicles of the OVB-organoids contain RPE in the outer layer of the vesicle. Especially the localization of the RPE-specific marker RPE65, and the hexagonal cell pattern of the actin cytoskeleton revealed by phalloidin and ZO-1 support the conclusion. However, the lack of *GJA1* and *CLDN19* expression combined with the localization of CI-19 outside the RPE would indicate that the RPE present in the vesicles is not mature by the 60-day timepoint.

To increase the yield of organoids developing optic vesicles, optimization of the original culturing protocol for specifically hESCs is recommended. For proper RPE maturation analyses, the RPE should be extracted from the OVB-organoids and individually cultured further. By comparing the structure and functionality of the organoid-grown RPE to 2D RPE, the influence of the neural retina on the maturity of the RPE grown in the OVB-organoids could be better assessed. Overall, the aims set for the thesis were met. The OVB-organoid protocol has its' challenges, but the results show promise and thus the protocol should be tested and developed further.

# REFERENCES


Aisenbrey, E.A., Murphy, W.L., 2020. Synthetic alternatives to Matrigel. Nat Rev Mater 5, 539–551. https://doi.org/10.1038/s41578-020-0199-8

Akhtar, T., Xie, H., Khan, M.I., Zhao, H., Bao, J., Zhang, M., Xue, T., 2019. Accelerated photoreceptor differentiation of hiPSC-derived retinal organoids by contact co-culture with retinal pigment epithelium. Stem Cell Research 39, 101491. https://doi.org/10.1016/j.scr.2019.101491

Alberts, B., Johnson, A., Lewis, J., Morgan, D., Raff, M., Roberts, K., Walter, P., 2015. Chapter 19: Cell Junctions and the Extracellular Matrix, in: Molecular Biology of the Cell. Garland Science, New York.

Almedawar, S., Vafia, K., Schreiter, S., Neumann, K., Khattak, S., Kurth, T., Ader, M., Karl, M.O., Tsang, S.H., Tanaka, E.M., 2020. MERTK-Dependent Ensheathment of Photoreceptor Outer Segments by Human Pluripotent Stem Cell-Derived Retinal Pigment Epithelium. Stem Cell Reports 14, 374–389. https://doi.org/10.1016/j.stemcr.2020.02.004

Alsanie, W.F., Niclis, J.C., Petratos, S., 2013. Human Embryonic Stem Cell-Derived Oligodendrocytes: Protocols and Perspectives. Stem Cells and Development 22, 2459–2476. https://doi.org/10.1089/scd.2012.0520

Angulo-Urarte, A., van der Wal, T., Huveneers, S., 2020. Cell-cell junctions as sensors and transducers of mechanical forces. Biochimica et Biophysica Acta (BBA) - Biomembranes 1862, 183316. https://doi.org/10.1016/j.bbamem.2020.183316

Arikawa, K., Williams, D.S., 1991. Alpha-actinin and actin in the outer retina: A double immunoelectron microscopic study. Cell Motility 18, 15–25. https://doi.org/10.1002/cm.970180103

Barral, D.C., Seabra, M.C., 2004. The Melanosome as a Model to Study Organelle Motility in Mammals. Pigment Cell Research 17, 111–118. https://doi.org/10.1111/j.1600-0749.2004.00138.x

Belova, L., Lavrov, A., Smirnikhina, S., 2022. Organoid transduction using recombinant adeno-associated viral vectors: Challenges and opportunities. BioEssays 44, 2200055. https://doi.org/10.1002/bies.202200055

Biesemeier, A., Schraermeyer, U., Eibl, O., 2011. Chemical composition of melanosomes, lipofuscin and melanolipofuscin granules of human RPE tissues. Experimental Eye Research 93, 29–39. https://doi.org/10.1016/j.exer.2011.04.004

Blenkinsop, T.A., Salero, E., Stern, J.H., Temple, S., 2013. The culture and maintenance of functional retinal pigment epithelial monolayers from adult human eye. Methods Mol Biol 945, 45–65. https://doi.org/10.1007/978-1-62703-125-7_4

Bonilha, V.L., 2014. Retinal pigment epithelium (RPE) cytoskeleton in vivo and in vitro. Experimental Eye Research, Retinal pigment epithelial cell culture: Current standards and technical criteria for model systems 126, 38–45. https://doi.org/10.1016/j.exer.2013.09.015

Bonilha, V.L., Finnemann, S.C., Rodriguez-Boulan, E., 1999. Ezrin Promotes Morphogenesis of Apical Microvilli and Basal Infoldings in Retinal Pigment Epithelium. Journal of Cell Biology 147, 1533–1548. https://doi.org/10.1083/jcb.147.7.1533

Booij, J.C., Baas, D.C., Beisekeeva, J., Gorgels, T.G.M.F., Bergen, A.A.B., 2010. The dynamic nature of Bruch's membrane. Progress in Retinal and Eye Research 29, 1–18. https://doi.org/10.1016/j.preteyeres.2009.08.003

Boulton, M., Rozanowska, M., Rozanowski, B., Wess, T., 2004. The photoreactivity of ocular lipofuscin. Photochem Photobiol Sci 3, 759–764. https://doi.org/10.1039/b400108g

Brooks, M.J., Chen, H.Y., Kelley, R.A., Mondal, A.K., Nagashima, K., De Val, N., Li, T., Chaitankar, V., Swaroop, A., 2019. Improved Retinal Organoid Differentiation by Modulating Signaling Pathways Revealed by Comparative Transcriptome Analyses with Development In Vivo. Stem Cell Reports 13, 891–905. https://doi.org/10.1016/j.stemcr.2019.09.009

Capowski, E.E., Samimi, K., Mayerl, S.J., Phillips, M.J., Pinilla, I., Howden, S.E., Saha, J., Jansen, A.D., Edwards, K.L., Jager, L.D., Barlow, K., Valiauga, R., Erlichman, Z., Hagstrom, A., Sinha, D., Sluch, V.M., Chamling, X., Zack, D.J., Skala, M.C., Gamm, D.M., 2019. Reproducibility and staging of 3D human retinal organoids across multiple pluripotent stem cell lines. Development (Cambridge, England) 146. https://doi.org/10.1242/dev.171686

Cepko, C., 2014. Intrinsically different retinal progenitor cells produce specific types of progeny. Nat Rev Neurosci 15, 615–627. https://doi.org/10.1038/nrn3767

Chen, G., Gulbranson, D.R., Hou, Z., Bolin, J.M., Ruotti, V., Probasco, M.D., Smuga-Otto, K., Howden, S.E., Diol, N.R., Propson, N.E., Wagner, R., Lee, G.O., Antosiewicz-Bourget, J., Teng, J.M.C., Thomson, J.A., 2011. Chemically defined conditions for human iPSC derivation and culture. Nat Methods 8, 424–429. https://doi.org/10.1038/nmeth.1593

Chen, G., Ushida, T., Tateishi, T., 2002. Scaffold Design for Tissue Engineering. Macromolecular Bioscience 2, 67–77. https://doi.org/10.1002/1616-5195(20020201)2:2<67::AID-MABI67>3.0.CO;2-F

Chen, S., Einspanier, R., Schoen, J., 2015. Transepithelial electrical resistance (TEER): a functional parameter to monitor the quality of oviduct epithelial cells cultured on filter supports. Histochem Cell Biol 144, 509–515. https://doi.org/10.1007/s00418-015-1351-1

Cook, J., Radu, R., Sun, H., Travis, G., 2013. Functional Characterization of Peropsin in the Retinal Pigment Epithelium. Investigative Ophthalmology & Visual Science 54, 3764.

Cornacchia, D., Zhang, C., Zimmer, B., Chung, S.Y., Fan, Y., Soliman, M.A., Tchieu, J., Chambers, S.M., Shah, H., Paull, D., Konrad, C., Vincendeau, M., Noggle, S.A., Manfredi, G., Finley, L.W.S., Cross, J.R., Betel, D., Studer, L., 2019. Lipid Deprivation Induces a Stable, Naive-to-Primed Intermediate State of Pluripotency in Human PSCs. Cell Stem Cell 25, 120-136.e10. https://doi.org/10.1016/j.stem.2019.05.001

Cowan, C.S., Renner, M., De Gennaro, M., Gross-Scherf, B., Goldblum, D., Hou, Y., Munz, M., Rodrigues, T.M., Krol, J., Szikra, T., Cuttat, R., Waldt, A., Papasaikas, P., Diggelmann, R., Patino-Alvarez, C.P., Galliker, P., Spirig, S.E., Pavlinic, D., Gerber-Hollbach, N., Schuierer, S., Srdanovic, A., Balogh, M., Panero, R., Kusnyerik, A., Szabo, A., Stadler, M.B., Orgül, S., Picelli, S., Hasler, P.W., Hierlemann, A., Scholl, H.P.N., Roma, G., Nigsch, F., Roska, B., 2020. Cell Types of the Human Retina and Its Organoids at Single-Cell Resolution. Cell 182, 1623-1640.e34. https://doi.org/10.1016/j.cell.2020.08.013

Cvekl, A., Wang, W.-L., 2009. Retinoic acid signaling in mammalian eye development. Experimental Eye Research 89, 280–291. https://doi.org/10.1016/j.exer.2009.04.012

Diacou, R., Nandigrami, P., Fiser, A., Liu, W., Ashery-Padan, R., Cvekl, A., 2022. Cell fate decisions, transcription factors and signaling during early retinal development. Progress in Retinal and Eye Research 101093. https://doi.org/10.1016/j.preteyeres.2022.101093

Eiraku, M., Takata, N., Ishibashi, H., Kawada, M., Sakakura, E., Okuda, S., Sekiguchi, K., Adachi, T., Sasai, Y., 2011. Self-organizing optic-cup morphogenesis in three-dimensional culture. Nature 472, 51–56. https://doi.org/10.1038/nature09941

Engelmann, K., Valtink, M., 2004. RPE cell cultivation. Graefe's Arch Clin Exp Ophthalmol 242, 65–67. https://doi.org/10.1007/s00417-003-0811-9

Erceg, S., Laínez, S., Ronaghi, M., Stojkovic, P., Pérez-Aragó, M.A., Moreno-Manzano, V., Moreno-Palanques, R., Planells-Cases, R., Stojkovic, M., 2008. Differentiation of Human Embryonic Stem Cells to Regional Specific Neural Precursors in Chemically Defined Medium Conditions. PLOS ONE 3, e2122. https://doi.org/10.1371/journal.pone.0002122

Esumi, N., Kachi, S., Hackler, L., Jr, Masuda, T., Yang, Z., Campochiaro, P.A., Zack, D.J., 2009. BEST1 expression in the retinal pigment epithelium is modulated by OTX family members. Human Molecular Genetics 18, 128–141. https://doi.org/10.1093/hmg/ddn323

Fadjukov, J., Wienbar, S., Hakanen, S., Aho, V., Vihinen-Ranta, M., Ihalainen, T.O., Schwartz, G.W., Nymark, S., 2022. Gap junctions and connexin hemichannels both contribute to the electrical properties of retinal pigment epithelium. J Gen Physiol 154, e202112916. https://doi.org/10.1085/jgp.202112916

Fahim, A., 2018. Retinitis pigmentosa: recent advances and future directions in diagnosis and management. Current Opinion in Pediatrics 30, 725. https://doi.org/10.1097/MOP.0000000000000690

Feldman, T.B., Dontsov, A.E., Yakovleva, M.A., Ostrovsky, M.A., 2022. Photobiology of lipofuscin granules in the retinal pigment epithelium cells of the eye: norm, pathology, age. Biophys Rev 14, 1051–1065. https://doi.org/10.1007/s12551-022-00989-9

Fligor, C.M., Langer, K.B., Sridhar, A., Ren, Y., Shields, P.K., Edler, M.C., Ohlemacher, S.K., Sluch, V.M., Zack, D.J., Zhang, C., Suter, D.M., Meyer, J.S., 2018. Three-Dimensional Retinal Organoids Facilitate the Investigation of Retinal Ganglion Cell Development, Organization and Neurite Outgrowth from Human Pluripotent Stem Cells. Sci Rep 8, 14520. https://doi.org/10.1038/s41598-018-32871-8

Fujimura, N., Taketo, M.M., Mori, M., Korinek, V., Kozmik, Z., 2009. Spatial and temporal regulation of Wnt/β-catenin signaling is essential for development of the retinal pigment epithelium. Developmental Biology 334, 31–45. https://doi.org/10.1016/j.ydbio.2009.07.002

Gabriel, E., Albanna, W., Pasquini, G., Ramani, A., Josipovic, N., Mariappan, A., Schinzel, F., Karch, C.M., Bao, G., Gottardo, M., Suren, A.A., Hescheler, J., Nagel-Wolfrum, K., Persico, V., Rizzoli, S.O., Altmüller, J., Riparbelli, M.G., Callaini, G., Goureau, O., Papantonis, A., Busskamp, V., Schneider, T., Gopalakrishnan, J., 2021. Human brain organoids assemble functionally integrated bilateral optic vesicles. Cell Stem Cell 28, 1740-1757.e8. https://doi.org/10.1016/j.stem.2021.07.010

Gallemore, R.P., Hughes, B.A., Miller, S.S., 1997. Retinal pigment epithelial transport mechanisms and their contributions to the electroretinogram. Progress in Retinal and Eye Research 16, 509–566. https://doi.org/10.1016/S1350-9462(96)00037-7

Gibbs, D., Williams, D.S., 2003. Isolation and Culture of Primary Mouse Retinal Pigmented Epithelial Cells, in: LaVail, M.M., Hollyfield, J.G., Anderson, R.E. (Eds.), Retinal Degenerations, Advances in Experimental Medicine and Biology. Springer US, Boston, MA, pp. 347–352. https://doi.org/10.1007/978-1-4615-0067-4_44

Goldberg, A.F.X., Moritz, O.L., Williams, D.S., 2016. Molecular basis for photoreceptor outer segment architecture. Progress in Retinal and Eye Research 55, 52–81. https://doi.org/10.1016/j.preteyeres.2016.05.003

Hartong, D.T., Berson, E.L., Dryja, T.P., 2006. Retinitis pigmentosa. The Lancet 368, 1795–1809. https://doi.org/10.1016/S0140-6736(06)69740-7

Hazim, R.A., Karumbayaram, S., Jiang, M., Dimashkie, A., Lopes, V.S., Li, D., Burgess, B.L., Vijayaraj, P., Alva-Ornelas, J.A., Zack, J.A., Kohn, D.B., Gomperts, B.N., Pyle, A.D., Lowry, W.E., Williams, D.S., 2017. Differentiation of RPE cells from integration-free iPS cells and their cell biological characterization. Stem Cell Res Ther 8, 217. https://doi.org/10.1186/s13287-017-0652-9

Hellinen, L., Sato, K., Reinisalo, M., Kidron, H., Rilla, K., Tachikawa, M., Uchida, Y., Terasaki, T., Urtti, A., 2019. Quantitative Protein Expression in the Human Retinal Pigment Epithelium: Comparison Between Apical and Basolateral Plasma Membranes With Emphasis on Transporters. Investigative Ophthalmology & Visual Science 60, 5022–5034. https://doi.org/10.1167/iovs.19-27328

Hey, C.A.B., Saltõkova, K.B., Bisgaard, H.C., Møller, L.B., 2018. Comparison of two different culture conditions for derivation of early hiPSC. Cell Biology International 42, 1467–1473. https://doi.org/10.1002/cbin.10966

Hongisto, H., Ilmarinen, T., Vattulainen, M., Mikhailova, A., Skottman, H., 2017. Xeno- and feeder-free differentiation of human pluripotent stem cells to two distinct ocular epithelial cell types using simple modifications of one method. Stem Cell Res Ther 8, 291. https://doi.org/10.1186/s13287-017-0738-4

Ishida, K., Panjwani, N., Cao, Z., Streilein, J.W., 2003. Participation of pigment epithelium in ocular immune privilege. 3. Epithelia cultured from iris, ciliary body, and retina suppress T-cell activation by partially non-overlapping mechanisms. Ocul Immunol Inflamm 11, 91–105. https://doi.org/10.1076/ocii.11.2.91.15914

Ishikawa, M., Sawada, Y., Yoshitomi, T., 2015. Structure and function of the interphotoreceptor matrix surrounding retinal photoreceptor cells. Experimental Eye Research, Ocular extracellular matrix: Role in development, homeostasis and disease 133, 3–18. https://doi.org/10.1016/j.exer.2015.02.017

Isla-Magrané, H., Veiga, A., García-Arumí, J., Duarri, A., 2021. Multiocular organoids from human induced pluripotent stem cells displayed retinal, corneal, and retinal pigment epithelium lineages. Stem Cell Res Ther 12, 581. https://doi.org/10.1186/s13287-021-02651-9

James, D., Levine, A.J., Besser, D., Hemmati-Brivanlou, A., 2005. TGFbeta/activin/nodal signaling is necessary for the maintenance of pluripotency in human embryonic stem cells. Development 132, 1273–1282. https://doi.org/10.1242/dev.01706

Janesick, A., Wu, S.C., Blumberg, B., 2015. Retinoic acid signaling and neuronal differentiation. Cell. Mol. Life Sci. 72, 1559–1576. https://doi.org/10.1007/s00018-014-1815-9

Janssen-Bienhold, U., Dermietzel, R., Weiler, R., 1998. Distribution of connexin43 immunoreactivity in the retinas of different vertebrates. J Comp Neurol 396, 310–321.

Jeong, S., An, B., Kim, J.-H., Han, H.-W., Kim, J.-H., Heo, H.-R., Ha, K.-S., Han, E.-T., Park, W.S., Hong, S.-H., 2020. BMP4 and perivascular cells promote hematopoietic differentiation of human pluripotent stem cells in a differentiation stage-specific manner. Exp Mol Med 52, 56–65. https://doi.org/10.1038/s12276-019-0357-5

Johansson, J.K., Karema-Jokinen, V.I., Hakanen, S., Jylhä, A., Uusitalo, H., Vihinen-Ranta, M., Skottman, H., Ihalainen, T.O., Nymark, S., 2019. Sodium channels enable fast electrical signaling and regulate phagocytosis in the retinal pigment epithelium. BMC Biol 17, 63. https://doi.org/10.1186/s12915-019-0681-1

Kaempf, S., Walter, P., Salz, A.K., Thumann, G., 2008. Novel organotypic culture model of adult mammalian neurosensory retina in co-culture with retinal pigment epithelium. Journal of Neuroscience Methods 173, 47–58. https://doi.org/10.1016/j.jneumeth.2008.05.018

Kay, P., Yang, Y.C., Paraoan, L., 2013. Directional protein secretion by the retinal pigment epithelium: roles in retinal health and the development of age-related macular degeneration. Journal of Cellular and Molecular Medicine 17, 833–843. https://doi.org/10.1111/jcmm.12070

Kennedy, C., Rakoczy, P., Constable, I., 1995. Lipofuscin of the retinal pigment epithelium: a review - PubMed. Eye (Lond) 9, 763–71. https://doi.org/10.1038/eye.1995.192

Kevany, B.M., Palczewski, K., 2010. Phagocytosis of Retinal Rod and Cone Photoreceptors. Physiology 25, 8–15. https://doi.org/10.1152/physiol.00038.2009

Khristov, V., Wan, Q., Sharma, R., Lotfi, M., Maminishkis, A., Bharti, K., 2018. Polarized Human Retinal Pigment Epithelium Exhibits Distinct Surface Proteome on Apical and Basal Plasma Membranes. Methods Mol Biol 1722, 223–247. https://doi.org/10.1007/978-1-4939-7553-2_15

Kiser, P.D., 2022. Retinal pigment epithelium 65 kDa protein (RPE65): An update. Progress in Retinal and Eye Research 88, 101013. https://doi.org/10.1016/j.preteyeres.2021.101013

Kiser, P.D., Golczak, M., Palczewski, K., 2014. Chemistry of the Retinoid (Visual) Cycle. Chem. Rev. 114, 194–232. https://doi.org/10.1021/cr400107q

Kivelä, T., Jääskeläinen, J., Vaheri, A., Carpén, O., 2000. Ezrin, a membrane-organizing protein, as a polarization marker of the retinal pigment epithelium in vertebrates. Cell Tissue Res 301, 217–223. https://doi.org/10.1007/s004410000225

Kolb, H., 2012. Photoreceptors, Webvision: The Organization of the Retina and Visual System [Internet]. University of Utah Health Sciences Center.

Kolb, H., 2007a. Outer Plexiform Layer, Webvision: The Organization of the Retina and Visual System [Internet]. University of Utah Health Sciences Center.

Kolb, H., 2007b. Roles of Amacrine Cells, Webvision: The Organization of the Retina and Visual System [Internet]. University of Utah Health Sciences Center.

Korkka, I., Viheriälä, T., Juuti-Uusitalo, K., Uusitalo-Järvinen, H., Skottman, H., Hyttinen, J., Nymark, S., 2018. Functional Voltage-Gated Calcium Channels Are Present in Human Embryonic Stem Cell-Derived Retinal Pigment Epithelium. Stem Cells Transl Med 8, 179–193. https://doi.org/10.1002/sctm.18-0026

Kwon, W., Freeman, S.A., 2020. Phagocytosis by the Retinal Pigment Epithelium: Recognition, Resolution, Recycling. Frontiers in Immunology 11.

Lakkaraju, A., Umapathy, A., Tan, L.X., Daniele, L., Philp, N.J., Boesze-Battaglia, K., Williams, D.S., 2020. The cell biology of the retinal pigment epithelium. Prog Retin Eye Res 100846. https://doi.org/10.1016/j.preteyeres.2020.100846

Lancaster, M.A., Knoblich, J.A., 2014. Organogenesis in a dish: modeling development and disease using organoid technologies. Science 345, 1247125. https://doi.org/10.1126/science.1247125

Lehmann, G.L., Benedicto, I., Philp, N.J., Rodriguez-Boulan, E., 2014. Plasma membrane protein polarity and trafficking in RPE cells: Past, present and future. Experimental Eye Research, Retinal pigment epithelial cell culture: Current standards and technical criteria for model systems 126, 5–15. https://doi.org/10.1016/j.exer.2014.04.021

Lei, Y., Jeong, D., Xiao, J., Schaffer, D.V., 2014. Developing Defined and Scalable 3D Culture Systems for Culturing Human Pluripotent Stem Cells at High Densities. Cel. Mol. Bioeng. 7, 172–183. https://doi.org/10.1007/s12195-014-0333-z

Li, X., Zhang, L., Tang, F., Wei, X., 2021. Retinal Organoids: Cultivation, Differentiation, and Transplantation. Front Cell Neurosci 15, 638439. https://doi.org/10.3389/fncel.2021.638439

Liu, H., Jing, L., Sun, J., Huang, D., 2021. An Overview of Scaffolds for Retinal Pigment Epithelium Research. Procedia Manufacturing, 49th SME North American Manufacturing Research Conference (NAMRC 49, 2021) 53, 492–499. https://doi.org/10.1016/j.promfg.2021.06.051

Ludwig, T.E., Bergendahl, V., Levenstein, M.E., Yu, J., Probasco, M.D., Thomson, J.A., 2006. Feeder-independent culture of human embryonic stem cells. Nat Methods 3, 637–646. https://doi.org/10.1038/nmeth902

Luo, Y., Zhuo, Y., Fukuhara, M., Rizzolo, L.J., 2006. Effects of culture conditions on heterogeneity and the apical junctional complex of the ARPE-19 cell line. Invest Ophthalmol Vis Sci 47, 3644–3655. https://doi.org/10.1167/iovs.06-0166

Lynn, S.A., Keeling, E., Dewing, J.M., Johnston, D.A., Page, A., Cree, A.J., Tumbarello, D.A., Newman, T.A., Lotery, A.J., Ratnayaka, J.A., 2018. A convenient protocol for establishing a human cell culture model of the outer retina. F1000Res 7, 1107. https://doi.org/10.12688/f1000research.15409.1

Ma, X., Li, H., Chen, Y., Yang, J., Chen, H., Arnheiter, H., Hou, L., 2019. The transcription factor MITF in RPE function and dysfunction. Progress in Retinal and Eye Research 73, 100766. https://doi.org/10.1016/j.preteyeres.2019.06.002

MacDonald, P.N., Ong, D.E., 1988. A lecithin:retinol acyltransferase activity in human and rat liver. Biochem Biophys Res Commun 156, 157–163. https://doi.org/10.1016/s0006-291x(88)80818-0

MacDuffie, K.E., Hyun, I., Krogen, M.M., Dempsey, J.C., Murry, C.E., Copp, A.J., Glass, I.A., Doherty, D., 2021. Rescuing human fetal tissue research in the United States: A call for additional regulatory reform. Stem Cell Reports 16, 2839–2843. https://doi.org/10.1016/j.stemcr.2021.10.016

Maminishkis, A., Chen, S., Jalickee, S., Banzon, T., Shi, G., Wang, F.E., Ehalt, T., Hammer, J.A., Miller, S.S., 2006. Confluent Monolayers of Cultured Human Fetal Retinal Pigment Epithelium Exhibit Morphology and Physiology of Native Tissue. Invest Ophthalmol Vis Sci 47, 3612–3624. https://doi.org/10.1167/iovs.05-1622

Mannagh, J., Arya, D.V., Irvine, A.R., Jr., 1973. Tissue culture of human retinal pigment epithelium. Investigative Ophthalmology & Visual Science 12, 52–64.

Marmorstein, A.D., 2001. The Polarity of the Retinal Pigment Epithelium. Traffic 2, 867–872. https://doi.org/10.1034/j.1600-0854.2001.21202.x

Marmorstein, A.D., Marmorstein, L.Y., Rayborn, M., Wang, X., Hollyfield, J.G., Petrukhin, K., 2000. Bestrophin, the product of the Best vitelliform macular dystrophy gene (VMD2), localizes to the basolateral plasma membrane of the retinal pigment epithelium. Proc Natl Acad Sci U S A 97, 12758–12763. https://doi.org/10.1073/pnas.220402097

Masaeli, E., Forster, V., Picaud, S., Karamali, F., Nasr-Esfahani, M.H., Marquette, C., 2020. Tissue engineering of retina through high resolution 3-dimensional inkjet bioprinting. Biofabrication 12, 025006. https://doi.org/10.1088/1758-5090/ab4a20

Masaeli, E., Marquette, C., 2020. Direct-Write Bioprinting Approach to Construct Multilayer Cellular Tissues. Frontiers in Bioengineering and Biotechnology 7.

Mata, N.L., Radu, R.A., Clemmons, R.S., Travis, G.H., 2002. Isomerization and Oxidation of Vitamin A in Cone-Dominant Retinas: A Novel Pathway for Visual-Pigment Regeneration in Daylight. Neuron 36, 69–80. https://doi.org/10.1016/S0896-6273(02)00912-1

May-Simera, H.L., Wan, Q., Jha, B.S., Hartford, J., Khristov, V., Dejene, R., Chang, J., Patnaik, S., Lu, Q., Banerjee, P., Silver, J., Insinna-Kettenhofen, C., Patel, D., Lotfi, M., Malicdan, M., Hotaling, N., Maminishkis, A., Sridharan, R., Brooks, B., Miyagishima, K., Gunay-Aygun, M., Pal, R., Westlake, C., Miller, S., Sharma, R., Bharti, K., 2018. Primary Cilium-Mediated Retinal Pigment Epithelium Maturation Is Disrupted in Ciliopathy Patient Cells. Cell Reports 22, 189–205. https://doi.org/10.1016/j.celrep.2017.12.038

Miller, S.S., Steinberg, R.H., Oakley, B., 1978. The electrogenic sodium pump of the frog retinal pigment epithelium. J Membr Biol 44, 259–279. https://doi.org/10.1007/BF01944224

Moiseyev, G., Chen, Y., Takahashi, Y., Wu, B.X., Ma, J., 2005. RPE65 is the isomerohydrolase in the retinoid visual cycle. Proceedings of the National Academy of Sciences 102, 12413–12418. https://doi.org/10.1073/pnas.0503460102

Morimura, H., Fishman, G.A., Grover, S.A., Fulton, A.B., Berson, E.L., Dryja, T.P., 1998. Mutations in the RPE65 gene in patients with autosomal recessive retinitis pigmentosa or leber congenital amaurosis. Proc Natl Acad Sci U S A 95, 3088–3093. https://doi.org/10.1073/pnas.95.6.3088

Morizane, A., Doi, D., Kikuchi, T., Nishimura, K., Takahashi, J., 2011. Small-molecule inhibitors of bone morphogenic protein and activin/nodal signals promote highly efficient neural induction from human pluripotent stem cells. J Neurosci Res 89, 117–126. https://doi.org/10.1002/jnr.22547

Nabi, I.R., Mathews, A.P., Cohen-Gould, L., Gundersen, D., Rodriguez-Boulan, E., 1993. Immortalization of polarized rat retinal pigment epithelium. J Cell Sci 104 ( Pt 1), 37–49. https://doi.org/10.1242/jcs.104.1.37

Nakano, T., Ando, S., Takata, N., Kawada, M., Muguruma, K., Sekiguchi, K., Saito, K., Yonemura, S., Eiraku, M., Sasai, Y., 2012. Self-Formation of Optic Cups and Storable Stratified Neural Retina from Human ESCs. Cell Stem Cell 10, 771–785. https://doi.org/10.1016/j.stem.2012.05.009

Narsinh, K.H., Plews, J., Wu, J.C., 2011. Comparison of Human Induced Pluripotent and Embryonic Stem Cells: Fraternal or Identical Twins? Mol Ther 19, 635–638. https://doi.org/10.1038/mt.2011.41

Nashine, S., 2021. Potential Therapeutic Candidates for Age-Related Macular Degeneration (AMD). Cells 10, 2483. https://doi.org/10.3390/cells10092483

Newman, E., Reichenbach, A., 1996. The Müller cell: a functional element of the retina. Trends Neurosci 19, 307–312. https://doi.org/10.1016/0166-2236(96)10040-0

Oswald, J., Baranov, P., 2018. Regenerative medicine in the retina: from stem cells to cell replacement therapy. Therapeutic Advances in Ophthalmology 10, 251584141877443. https://doi.org/10.1177/2515841418774433

Otani, T., Furuse, M., 2020. Tight Junction Structure and Function Revisited. Trends in Cell Biology 30, 805–817. https://doi.org/10.1016/j.tcb.2020.08.004

Patel, R., Alahmad, A.J., 2016. Growth-factor reduced Matrigel source influences stem cell derived brain microvascular endothelial cell barrier properties. Fluids and Barriers of the CNS 13, 6. https://doi.org/10.1186/s12987-016-0030-5

Peng, S., Wang, S.B., Singh, D., Zhao, P.Y.C., Davis, K., Chen, B., Adelman, R.A., Rizzolo, L.J., 2016. Claudin-3 and claudin-19 partially restore native phenotype to ARPE-19 cells via effects on tight junctions and gene expression. Experimental eye research 151, 179–189. https://doi.org/10.1016/j.exer.2016.08.021

Pera, M.F., Reubinoff, B., Trounson, A., 2000. Human embryonic stem cells. Journal of Cell Science 113, 5–10. https://doi.org/10.1242/jcs.113.1.5

Prado, D.A., Acosta-Acero, M., Maldonado, R.S., 2020. Gene therapy beyond luxturna: a new horizon of the treatment for inherited retinal disease. Current Opinion in Ophthalmology 31, 147. https://doi.org/10.1097/ICU.0000000000000660

Prakash Bangalore, M., Adhikarla, S., Mukherjee, O., Panicker, M.M., 2017. Genotoxic Effects of Culture Media on Human Pluripotent Stem Cells. Sci Rep 7, 42222. https://doi.org/10.1038/srep42222

Rambhatla, L., Chiu, C.-P., Glickman, R.D., Rowe-Rendleman, C., 2002. In vitro differentiation capacity of telomerase immortalized human RPE cells. Invest Ophthalmol Vis Sci 43, 1622–1630.

Rando, R.R., 2001. The Biochemistry of the Visual Cycle. Chem. Rev. 101, 1881–1896. https://doi.org/10.1021/cr960141c

Regent, F., Chen, H.Y., Kelley, R.A., Qu, Z., Swaroop, A., Li, T., 2020. A simple and efficient method for generating human retinal organoids. Mol Vis 26, 97–105. https://doi.org/PMCID: PMC7051860

Röhlich, P., 1970. The interphotoreceptor matrix: Electron microscopic and histochemical observations on the vertebrate retina. Experimental Eye Research 10, 80–86. https://doi.org/10.1016/S0014-4835(70)80013-6

Sadler, T.W., Langman, J., 2012. Langman's Medical Embryology: Chapter 20, 12th ed. ed. Wolters Kluwer Health/Lippincott Williams & Wilkins, Philadelphia.

Schindelin, J., Arganda-Carreras, I., Frise, E., Kaynig, V., Longair, M., Pietzsch, T., Preibisch, S., Rueden, C., Saalfeld, S., Schmid, B., Tinevez, J.-Y., White, D.J., Hartenstein, V., Eliceiri, K., Tomancak, P., Cardona, A., 2012. Fiji: an open-source platform for biological-image analysis. Nat Methods 9, 676–682. https://doi.org/10.1038/nmeth.2019

Schwab, I.R., 2011. Evolution's Witness: How Eyes Evolved. Oxford University Press, Incorporated, Oxford, UNITED STATES.

Selcan Gungor-Ozkerim, P., Inci, I., Shrike Zhang, Y., Khademhosseini, A., Remzi Dokmeci, M., 2018. Bioinks for 3D bioprinting: an overview. Biomaterials Science 6, 915–946. https://doi.org/10.1039/C7BM00765E

Sernagor, E., Eglen, S.J., Wong, R.O.L., 2001. Development of Retinal Ganglion Cell Structure and Function. Progress in Retinal and Eye Research 20, 139–174. https://doi.org/10.1016/S1350-9462(00)00024-0

Sheedlo, H.J., Nelson, T.H., Lin, N., Rogers, T.A., Roque, R.S., Turner, J.E., 1998. RPE secreted proteins and antibody influence photoreceptor cell survival and maturation. Developmental Brain Research 107, 57–69. https://doi.org/10.1016/S0165-3806(97)00219-8

Skottman, H., 2010. Derivation and characterization of three new human embryonic stem cell lines in Finland. In Vitro Cell.Dev.Biol.-Animal 46, 206–209. https://doi.org/10.1007/s11626-010-9286-2

Slavotinek, A.M., 2011. Eye development genes and known syndromes. Molecular Genetics and Metabolism 104, 448–456. https://doi.org/10.1016/j.ymgme.2011.09.029

Solano, F., 2014. Melanins: Skin Pigments and Much More—Types, Structural Models, Biological Functions, and Formation Routes. New Journal of Science 2014, 1–28. https://doi.org/10.1155/2014/498276

Somasundaran, S., Constable, I.J., Mellough, C.B., Carvalho, L.S., 2020. Retinal pigment epithelium and age-related macular degeneration: A review of major disease mechanisms. Clin Exp Ophthalmol 48, 1043–1056. https://doi.org/10.1111/ceo.13834

Song, M.J., Quinn, R., Nguyen, E., Hampton, C., Sharma, R., Park, T.S., Koster, C., Voss, T., Tristan, C., Weber, C., Singh, A., Dejene, R., Bose, D., Chen, Y.-C., Derr, P., Derr, K., Michael, S., Barone, F., Chen, G., Boehm, M., Maminishkis, A., Singec, I., Ferrer, M., Bharti, K., 2023. Bioprinted 3D outer retina barrier uncovers RPE-dependent choroidal phenotype in advanced macular degeneration. Nat Methods 20, 149–161. https://doi.org/10.1038/s41592-022-01701-1

Sonoda, S., Spee, C., Barron, E., Ryan, S.J., Kannan, R., Hinton, D.R., 2009. A protocol for the culture and differentiation of highly polarized human retinal pigment epithelial cells. Nat Protoc 4, 662–673. https://doi.org/10.1038/nprot.2009.33

Sosinsky, G.E., Nicholson, B.J., 2005. Structural organization of gap junction channels. Biochimica et Biophysica Acta (BBA) - Biomembranes, The Connexins Part II 1711, 99–125. https://doi.org/10.1016/j.bbamem.2005.04.001

Strauss, O., 2005. The Retinal Pigment Epithelium in Visual Function. Physiological Reviews 85, 845–881. https://doi.org/10.1152/physrev.00021.2004

Sun, C., Zhou, J., Meng, X., 2021. Primary cilia in retinal pigment epithelium development and diseases. Journal of Cellular and Molecular Medicine 25, 9084–9088. https://doi.org/10.1111/jcmm.16882

Sun, H., Gilbert, D.J., Copeland, N.G., Jenkins, N.A., Nathans, J., 1997. Peropsin, a novel visual pigment-like protein located in the apical microvilli of the retinal pigment epithelium. Proceedings of the National Academy of Sciences 94, 9893–9898. https://doi.org/10.1073/pnas.94.18.9893

Takahashi, K., Tanabe, K., Ohnuki, M., Narita, M., Ichisaka, T., Tomoda, K., Yamanaka, S., 2007. Induction of pluripotent stem cells from adult human fibroblasts by defined factors. Cell 131, 861–872. https://doi.org/10.1016/j.cell.2007.11.019

Tan, Y.S.E., Shi, P.J., Choo, C.-J., Laude, A., Yeong, W.Y., 2018. Tissue engineering of retina and Bruch's membrane: a review of cells, materials and processes. British Journal of Ophthalmology 102, 1182–1187. https://doi.org/10.1136/bjophthalmol-2017-311390

Terakita, A., 2005. The opsins. Genome Biol 6, 213. https://doi.org/10.1186/gb-2005-6-3-213

Thomas, B.B., Lin, B., Martinez-Camarillo, J.C., Zhu, D., McLelland, B.T., Nistor, G., Keirstead, H.S., Humayun, M.S., Seiler, M.J., 2021. Co-grafts of Human Embryonic Stem Cell Derived Retina Organoids and Retinal Pigment Epithelium for Retinal Reconstruction in Immunodeficient Retinal Degenerate Royal College of Surgeons Rats. Frontiers in Neuroscience 15.

Thomas, C.J., Mirza, R.G., Gill, M.K., 2021. Age-Related Macular Degeneration. Medical Clinics of North America 105, 473–491. https://doi.org/10.1016/j.mcna.2021.01.003

Timpl, R., Rohde, H., Robey, P.G., Rennard, S.I., Foidart, J.M., Martin, G.R., 1979. Laminin–a glycoprotein from basement membranes. Journal of Biological Chemistry 254, 9933–9937. https://doi.org/10.1016/S0021-9258(19)83607-4

Toops, K.A., Tan, L.X., Lakkaraju, A., 2014. A detailed three-step protocol for live imaging of intracellular traffic in polarized primary porcine RPE monolayers. Exp Eye Res 124, 74–85. https://doi.org/10.1016/j.exer.2014.05.003

Viheriälä, T., Hongisto, H., Sorvari, J., Skottman, H., Nymark, S., Ilmarinen, T., 2022. Cell maturation influences the ability of hESC-RPE to tolerate cellular stress. Stem Cell Res Ther 13, 30. https://doi.org/10.1186/s13287-022-02712-7

Völkner, M., Pavlou, M., Büning, H., Michalakis, S., Karl, M.O., 2021. Optimized Adeno-Associated Virus Vectors for Efficient Transduction of Human Retinal Organoids. Human Gene Therapy 32, 694–706. https://doi.org/10.1089/hum.2020.321

Wang, J.-S., Kefalov, V.J., 2011. The Cone-specific visual cycle. Progress in Retinal and Eye Research 30, 115–128. https://doi.org/10.1016/j.preteyeres.2010.11.001

Wang, P., Li, X., Zhu, W., Zhong, Z., Moran, A., Wang, W., Zhang, K., Chen, S., 2018. 3D bioprinting of hydrogels for retina cell culturing. Bioprinting 12, e00029. https://doi.org/10.1016/j.bprint.2018.e00029

Westenskow, P., Piccolo, S., Fuhrmann, S., 2009. β-catenin controls differentiation of the retinal pigment epithelium in the mouse optic cup by regulating Mitf and Otx2 expression. Development 136, 2505–2510. https://doi.org/10.1242/dev.032136

Wimmers, S., Karl, M.O., Strauss, O., 2007. Ion channels in the RPE. Prog Retin Eye Res 26, 263–301. https://doi.org/10.1016/j.preteyeres.2006.12.002

Wong, W.L., Su, X., Li, X., Cheung, C.M.G., Klein, R., Cheng, C.-Y., Wong, T.Y., 2014. Global prevalence of age-related macular degeneration and disease burden projection for 2020 and 2040: a systematic review and meta-analysis. The Lancet Global Health 2, e106–e116. https://doi.org/10.1016/S2214-109X(13)70145-1

Wu, W., Zeng, Y., Li, Z., Li, Q., Xu, H., Yin, Z.Q., 2016. Features specific to retinal pigment epithelium cells derived from three-dimensional human embryonic stem cell cultures — a new donor for cell therapy. Oncotarget 7, 22819–22833. https://doi.org/10.18632/oncotarget.8185

Xiang, P., Wu, K.-C., Zhu, Y., Xiang, L., Li, C., Chen, D.-L., Chen, F., Xu, G., Wang, A., Li, M., Jin, Z.-B., 2014. A novel Bruch's membrane-mimetic electrospun substrate scaffold for human retinal pigment epithelium cells. Biomaterials 35, 9777–9788. https://doi.org/10.1016/j.biomaterials.2014.08.040

Yamanaka, S., 2012. Induced Pluripotent Stem Cells: Past, Present, and Future. Cell Stem Cell 10, 678–684. https://doi.org/10.1016/j.stem.2012.05.005

Young, R.W., Bok, D., 1969. PARTICIPATION OF THE RETINAL PIGMENT EPITHELIUM IN THE ROD OUTER SEGMENT RENEWAL PROCESS. Journal of Cell Biology 42, 392–403. https://doi.org/10.1083/jcb.42.2.392

Zakrzewski, W., Dobrzyński, M., Szymonowicz, M., Rybak, Z., 2019. Stem cells: past, present, and future. Stem Cell Res Ther 10, 68. https://doi.org/10.1186/s13287-019-1165-5

Zerti, D., Dorgau, B., Felemban, M., Ghareeb, A.E., Yu, M., Ding, Y., Krasnogor, N., Lako, M., 2020. Developing a simple method to enhance the generation of cone and rod photoreceptors in pluripotent stem cell-derived retinal organoids. Stem Cells 38, 45–51. https://doi.org/10.1002/stem.3082

Zhang, Q., Chrenek, M.A., Bhatia, S., Rashid, A., Ferdous, S., Donaldson, K.J., Skelton, H., Wu, W., See, T.R.O., Jiang, Y., Dalal, N., Nickerson, J.M., Grossniklaus, H.E., 2019. Comparison of histologic findings in age-related macular degeneration with RPE flatmount images. Mol Vis 25, 70–78.

Zhang, X., Wang, W., Jin, Z.-B., 2021. Retinal organoids as models for development and diseases. Cell Regen 10, 33. https://doi.org/10.1186/s13619-021-00097-1

Zhong, X., Gutierrez, C., Xue, T., Hampton, C., Vergara, M.N., Cao, L.-H., Peters, A., Park, T.S., Zambidis, E.T., Meyer, J.S., Gamm, D.M., Yau, K.-W., Canto-Soler, M.V., 2014. Generation of three-dimensional retinal tissue with functional photoreceptors from human iPSCs. Nat Commun 5, 4047. https://doi.org/10.1038/ncomms5047

Zhou, J., Su, P., Li, D., Tsang, S., Duan, E., Wang, F., 2010. High-efficiency induction of neural conversion in human ESCs and human induced pluripotent stem cells with a single chemical inhibitor of transforming growth factor beta superfamily receptors. Stem Cells 28, 1741–1750. https://doi.org/10.1002/stem.504

Zielicka, Z., Williams, J.A.E., Moss, S.E., 2015. Gap junctions modulate the phagocytic activity of retinal pigment epithelial cells. Investigative Ophthalmology & Visual Science 56, 2322.

# SUPPLEMENTAL METHODS

***Supplemental Table 1.*** *The components of the Neurosphere culturing medium used in the neurosphere phase.*

| Component | Manufacturer | Final concentration |
|---|---|---|
| DMEM/F-12 | Thermo Fisher Scientific | 48.4 % (v/v) |
| Neurobasal™ Medium | Thermo Fisher Scientific | 48.4 % (v/v) |
| N-2 Supplement (100X) | Gibco™ | 0.4X |
| B-27™ Supplement (50X) without vitamin A | Gibco™ | 0.2X |
| Glutamax (100X) | Gibco™ | 1X |
| MEM NEAA (100X) | Gibco™ | 0.5X |
| Insulin Solution Human | Sigma Aldrich | 1 ml/l of medium |
| SB431542 (10 mM/1 ml) | Selleck Chemicals | 2.5 μM |
| Penicillin Streptomycin (10 000 U/ml) | Thermo Fisher Scientific | 100 U/ml |
| 2-Mercaptoethanol (50 mM) | Thermo Fisher Scientific | 5 μM |
| Matrigel | Corning | 0.1 % (v/v) |

***Supplemental table 2.*** *The components of the OVB culturing medium used in the organoid phase.*

| Component | Manufacturer | Final concentration |
|---|---|---|
| DMEM/F-12 | Thermo Fisher Scientific | 48.4 % (v/v) |
| Neurobasal™ Medium | Thermo Fisher Scientific | 48.4 % (v/v) |
| N-2 Supplement (100X) | Gibco™ | 0.4X |
| B-27 Supplement (50X) | Gibco™ | 0.2X |
| Glutamax (100X) | Gibco™ | 1X |
| MEM NEAA (100X) | Gibco™ | 0.5X |
| Insulin Solution Human | Sigma Aldrich | 1 ml/l of medium |
| SB431542 (10 mM/1 ml) | Selleck Chemicals | 2.5 μM |
| Penicillin Streptomycin (10 000 U/ml) | Thermo Fisher Scientific | 100 U/ml |
| 2-Mercaptoethanol (50 mM) | Thermo Fisher Scientific | 5 μM |
| Dorsomorphin in DMSO (5 mM) | STEMCELL™ Technologies | 0.5 μM |

***Supplemental Table 3.*** *The primer sequences for the gene expression analysis of the 20-day-old early-phase OVB-organoids. Product lengths are based on the information provided by the primer designer.*

| Gene | Forward primer sequence | Reverse primer sequence | Product length (bp) |
|---|---|---|---|
| *POU5F1* | CGTGAAGCTGGAGAAGGAGAAGCTG | AAGGGCCGCAGCTTACACATGTTC | 245 |
| *RAX* | CTGAAAGCCAAGGAGCACATC | CTCCTGGGAATGGCCAAGTTT | 409 |
| *PAX6* | AACAGACACAGCCCTCACAAACA | CGGGAACTTGAACTGGAACTGAC | 274 |
| *OTX2* | CATGCAGAGGTCCTATCCCAT | AAGCTGGGGACTGATTGAGAT | 200 |
| *SOX2* | GCCGAGTGGAAACTTTTGTCG | GGCAGCGTGTACTTATCCTTCT | 155 |
| *GAPDH* | GTTCGACAGTCAGCCGCATC | GGAATTTGCCATGGGTGGA | 229 |

***Supplemental Table 4.*** *The primer sequences for the gene expression analysis of the 50- and 60-day-old late-phase OVB-organoids. Product lengths are based on the information provided by the primer designer.*

| Gene | Forward primer sequence | Reverse primer sequence | Product length (bp) |
|---|---|---|---|
| *MITF* | TTGCAACGAGAACAGCAACG | ATGCTGAAGGAGGTCTTGGC | 225 |
| *RPE65* | CCATGGGGGTTTGGCTTCAT | TGGCAGTTGTATTGGGGAGC | 324 |
| *RRH* | TGGCCATCATAGCTCCACTG | CAGGACACAGAGAAGCATAC | 379 |
| *MERTK* | CGCTCTGGCGTAGAGCTATC | GTGTGTTTGAAGGCAAGAGGC | 250 |
| *CLDN19* | AGCAGTCTTCCTACGCAGG | CGCGCTGATTGGATGTGAC | 151 |
| *GJA1* | AATTCCAGCCCTGGTCTCAG | GTGAGGGCCAGCAGGTG | 300 |
| *CALB2* | ACTTTGACGCAGACGGAAATG | GAAGTTCTCTTCGGTTGGCAG | 215 |
| *GAD2* | TTTTGGTCTTTCGGGTCGGAA | TTCTCGGCGTCTCCGTAGAG | 140 |
| *GAP43* | GGCCGCAACCAAAATTCAGG | CGGCAGTAGTGGTGCCTTC | 167 |
| *RCVRN* | CCTCTACGACGTGGACGGTAA | GTGTTTTCATCGTCTGGAAGGA | 120 |

***Supplemental Table 5.*** *The primary antibodies used for the immunofluorescence stainings of the 60-day-old late-phase Matrigel-organoids.*

| Antibody | Dilution | Manufacturer |
|---|---|---|
| Mouse anti-CRALBP | 1:500 | Abcam |
| Mouse anti-Connexin 36 | 1:200 | Invitrogen |
| Mouse anti-Connexin 43 | 1:200 | Abcam |
| Mouse anti-Na/K-ATPase | 1:200 | Abcam |
| Mouse anti-Ezrin | 1:200 | Abcam |
| Mouse anti-Cl-19 | 1:100 | R&D (United States) |
| Mouse anti-Opsin | 1:200 | Sigma-Aldrich |
| Rabbit anti-PanNaV | 1:200 | Alomone labs (Israel) |
| Rabbit anti-ZO-1 | 1:200 | Invitrogen |
| Rabbit anti-RPE65 | 1:200 | GeneTex (United States) |

# SUPPLEMENTAL FIGURES

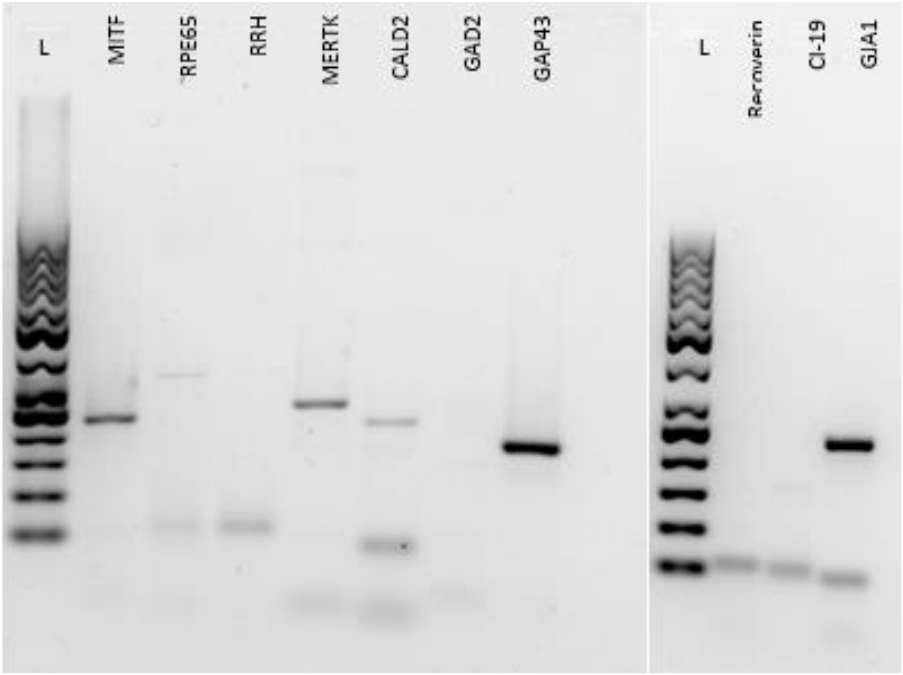


***Supplemental Figure 1**. 50-day-old late-phase Matrigel-organoids from a single batch (n total = 33, n with vesicles = 2). L = 50 bp GeneRuler ladder.*

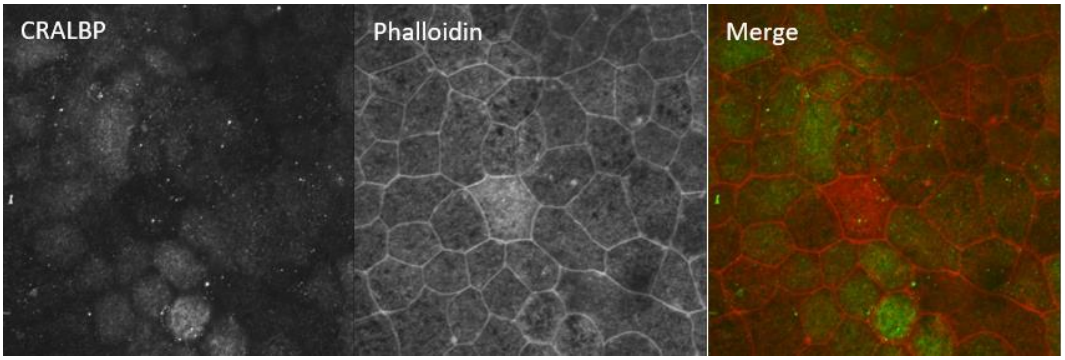


***Supplemental Figure 2**. Immunofluorescence stainings of 8-week-old 08/017 RPE insert with antibodies for CRALBP and phalloidin. In the merged image, CRALBP is green and phalloidin red. Imaged with the Zeiss Plan-Apochromat 63x/1.40 oil objective.*

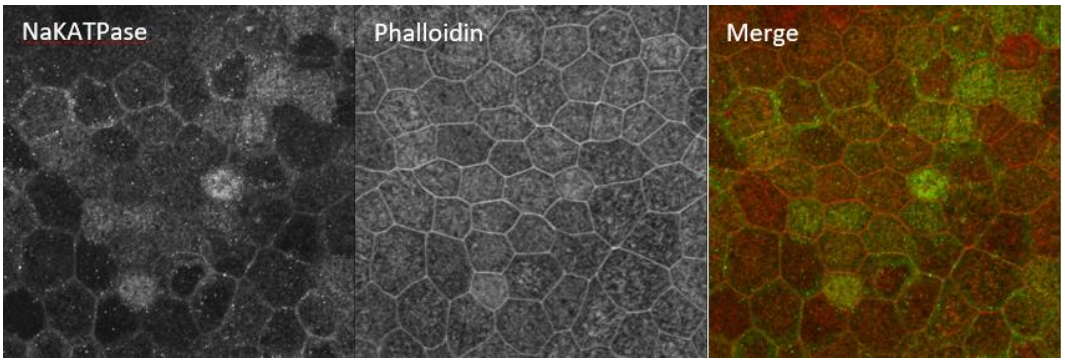


***Supplemental Figure 3**. Immunofluorescence stainings of 8-week-old 08/017 RPE insert with antibodies for Na/K-ATPase and phalloidin. In the merged image, Na/K-ATPase is green and phalloidin red. Imaged with the Zeiss Plan-Apochromat 63x/1.40 oil objective.*

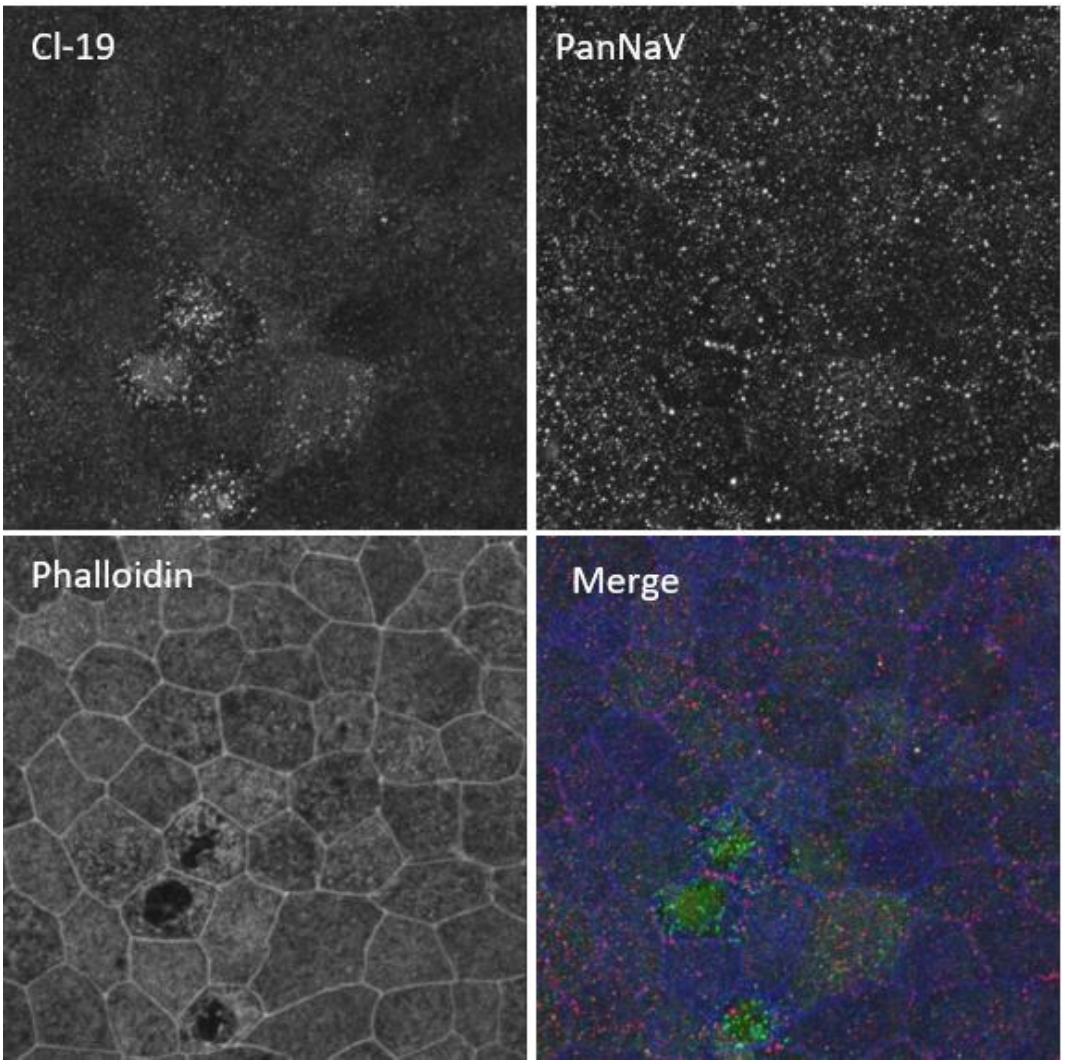


***Supplemental Figure 4**. Immunofluorescence stainings of 8-week-old 08/017 RPE insert with antibodies for Cl-19, PanNa$_V$ and phalloidin. In the merged image, Cl-19 is green, PanNa$_V$ red, and phalloidin blue. Imaged with the Zeiss Plan-Apochromat 63x/1.40 oil objective.*